

# Stochastic sampling effects favor manual over digital contact tracing

Marco Mancastropa,<sup>1,2</sup> Claudio Castellano,<sup>3</sup> Alessandro Vezzani,<sup>4,1</sup> and Raffaella Burioni<sup>1,2</sup>

<sup>1</sup>*Dipartimento di Scienze Matematiche, Fisiche e Informatiche,  
Università degli Studi di Parma, Parco Area delle Scienze, 7/A 43124 Parma, Italy*

<sup>2</sup>*INFN, Sezione di Milano Bicocca, Gruppo Collegato di Parma,  
Parco Area delle Scienze, 7/A 43124 Parma, Italy*

<sup>3</sup>*Istituto dei Sistemi Complessi (ISC-CNR), Via dei Taurini 19, I-00185 Roma, Italy*

<sup>4</sup>*Istituto dei Materiali per l'Elettronica ed il Magnetismo (IMEM-CNR),  
Parco Area delle Scienze, 37/A-43124 Parma, Italy*

(Dated: November 17, 2021)

Isolation of symptomatic individuals, together with tracing and testing of their nonsymptomatic contacts, is a fundamental strategy for mitigating the current COVID-19 pandemic before pharmaceutical interventions become available. The breaking of contagion chains relies on two main alternative strategies: manual reconstruction of contacts based on interviews or a digital (app-based) privacy-preserving contact tracing protocol. We compare in the same framework the effectiveness of the two strategies within the activity-driven model, a general empirically validated framework for network dynamics. Using model parameters tailored to describe SARS-CoV-2 diffusion, we show that even when the probability for a contact to be traced is the same, manual contact tracing robustly performs better than the digital protocol in increasing the epidemic threshold, limiting the height of the epidemic peaks and reducing the number of isolated individuals. This remains true even taking into account the intrinsic delay and limited scalability of the manual procedure. This result is explained in terms of the stochastic sampling occurring during the case-by-case manual reconstruction of contacts of infected individuals, contrasted with the intrinsically prearranged nature of digital tracing, determined by the decision to adopt the app or not of each individual. The better performance of manual tracing is enhanced by the heterogeneous features of agent behavior: a superspreader not adopting the app is completely invisible to digital contact tracing, while she can be traced manually, due to her multiple contacts. Our results indicate a careful integration of the two intrinsically different protocols as key to optimal mitigation strategies.

Keywords: Epidemics, Temporal networks, Contact tracing, Manual and digital contact tracing, COVID-19

The current COVID-19 pandemic is impacting daily life worldwide at an unprecedented scale. Among the features that have contributed to transform the emerging diffusion of SARS-CoV-2 coronavirus into such a global scale crisis, a prominent role is played by the high rates of virus transmission mediated by presymptomatic and asymptomatic individuals [1–6]. Given the absence of effective pharmaceutical interventions, this feature makes the mitigation of the pandemic a highly nontrivial task, that has been tackled with various strategies, none of them devoid of drawbacks.

Initially, governments resorted to very restrictive limitations of non strictly necessary activities (lock-downs) to curb the diffusion of the infection. Such measures turned out to be effective from an epidemiological point of view, but exceedingly costly in other respects, for their economic and social consequences [7, 8]. Recently, such restrictive measures have been progressively lifted, and we now rely on other tools to contain the pandemic: social distancing, reinforced hygiene and the use of individual protection devices. Along with these provisions, aimed at preventing single virus transmission events, another set of measures points at breaking contagion chains: the isolation of infected individuals (symptomatic or found via some testing), followed by the tracing of their contacts (contact tracing, CT), the testing of the latter and the possible isolation of the infected [9–12].

This CT procedure has proven effective in the past in various contexts [13–16] but it comes, in its standard manual implementation, with important limitations [17]. It requires the set up of a physical infrastructure, needed to find infected individuals, interview them and reconstruct their contacts in a temporal window, call these contacts, convince them to get tested and eventually isolated. Apart from the evident problems of practical feasibility and economic cost, the manual CT procedure intrinsically implies a delay between the moment an individual is found infected (and isolated) and the time her contacts are tested and possibly isolated. For an epidemic such as COVID-19, characterized by a rather long presymptomatic infectious stage and a high relevance of transmission by asymptomatics, the delay implied by manual CT risks to undermine the effectiveness of the whole procedure.

For this reason the alternative strategy of a digital CT procedure, based in particular on the installation of apps on smartphones (app-based), has been proposed [2]. The rationale is that proximity sensors installed on these ubiquitous devices allow the detection of contacts of epidemiological significance among individuals. When an individual is found infected, the app permits to instantaneously trace all contacts in the recent past, thus allowing for much quicker testing and isolation. A quantitative comparison between manual and digital CT applied to

an epidemiological model describing COVID-19 diffusion suggested that already a delay of the order of 3 days completely spoils the ability of manual CT to prevent the initial exponential growth of the epidemic [2]. The conclusion was that only a digital CT avoiding this delay could be a viable strategy to control the current epidemic. The proposal for digital CT rapidly gained momentum, leading to the development of technical solutions [18–20] and to the deployment of app-based CT infrastructures in many countries [21].

Many works have scrutinized the actual validity of this solution and investigated the possible shortcomings of app-based CT, casting doubts over many of the assumptions underlying such strategy [22–24]: there are too few modern enough smartphones; Bluetooth based proximity measurements are unreliable; co-location is not always a good proxy for epidemiological contact. The potential risks for privacy breaches have also been exposed.

Other papers have tried to evaluate the impact of digital CT on the current COVID-19 epidemic, attempting to precisely determine, by means of detailed data-driven epidemiological models, to what extent such a strategy is able to suppress virus diffusion [25–29]. A critical role is played by the fraction  $f$  of individuals in a population that actually use the app. Fairly high values of  $f$  (of the order of 60%) are required for the digital CT protocol to lead to global protection [2, 9, 23]. These values are in striking contrast with the low app adoption rates observed so far in most countries [30–32].

In this paper we take a different approach. We compare the effectiveness of the two CT protocols in exactly the same conditions, i.e., in the very same realistic epidemiological scenario, without making claims on their absolute performance. We consider a sensible epidemiological model incorporating all main ingredients of the current epidemic, with parameters tuned to values derived from empirical observations about COVID-19 spreading. Within this single framework we consider the impact of both manual and digital CT strategies, working in similar manner but with their own specific features: delayed isolation of contacts, limited scalability and imperfect recall for the manual procedure; dependence on the predetermined app adoption decision for the digital CT.

The comparison reveals that even when the number of reconstructed contacts is the same, manual CT performs better than digital CT in practically all realistic cases. The manual protocol is more efficient in increasing the epidemic threshold (i.e., the value of the effective infection rate above which the infection spreads diffusely), in limiting the height of the epidemic peaks and in reducing the number of isolated individuals. This surprising result is due to the stochastic *annealed* nature of the manual CT procedure, in which each symptomatic node randomly recalls a fraction of her contacts, in contrast with the digital CT where the traced nodes belong deterministically to the prearranged *quenched* fraction of the population adopting the app. In the latter case, the individuals not adopting the app can never be reached by the CT proto-

col, while the entire population is potentially detectable through the stochastic sampling of the manual procedure. The better performance of manual CT is already evident in homogeneous populations and it is strongly enhanced in the presence of a heterogeneous distribution of contacts. Superspreaders not adopting the app are invisible to the digital tracing while they are very likely to be detected by a manual tracing originating from one of their many contacts.

## I. RESULTS

### A. Epidemic spreading on heterogeneous dynamical networks

We consider an activity-driven network model with attractiveness, taking into account both the temporal dynamics of social contacts and the heterogeneity in the propensity to establish social ties [33–35]. Each susceptible node  $S$  is assigned with an activity  $a_S$  and an attractiveness parameter  $b_S$ , drawn from the joint distribution  $\rho(a_S, b_S)$ : the activation rate  $a_S$  describes the Poissonian activation dynamics of the node; the attractiveness  $b_S$  sets the probability  $p_{b_S} \propto b_S$  for a node to be contacted by an active agent. At the beginning all nodes are disconnected and when a node activates it creates  $m$  links with  $m$  randomly selected nodes (hereafter we set  $m = 1$ ); then all links are destroyed and the procedure is iterated. The functional form of  $\rho(a_S, b_S)$  encodes the correlations between activity and attractiveness in a population with a given distribution of activity. It has been observed that several social systems feature positive correlations between activity and attractiveness and a broad power-law distribution of activity [33–37]:

$$\rho_S(a_S, b_S) \sim a_S^{-(\nu+1)} \delta(b_S - a_S) \quad (1)$$

with  $\nu$  typically ranging between 0.5 and 2.

On top of the activity-driven dynamics, we consider a compartmental epidemic model which includes the main phases of clinical progression of the SARS-CoV-2 infection [6, 38–40], also applicable to other infectious diseases with asymptomatic and presymptomatic transmission. The model is composed by five compartments:  $S$  susceptible,  $P$  presymptomatic,  $A$  infected asymptomatic,  $I$  infected symptomatic,  $R$  recovered. A contagion process (see Fig. 1(a)) occurs with probability  $\lambda$  when a link is established between an infected (either  $P$ ,  $A$  and  $I$ ) and a susceptible node  $S$  (contact-driven transition): a node has probability  $\delta$  to become presymptomatic after infection and probability  $(1 - \delta)$  to become asymptomatic, thus  $S \xrightarrow{\lambda\delta} P$  and  $S \xrightarrow{\lambda(1-\delta)} A$ . A presymptomatic node spontaneously develops symptoms with rate  $\gamma_P = 1/\tau_P$ , thus with a Poissonian process  $P \xrightarrow{\gamma_P} I$ ; both asymptomatic and symptomatic nodes spontaneously recover respectively with rate  $\mu = 1/\tau$  and

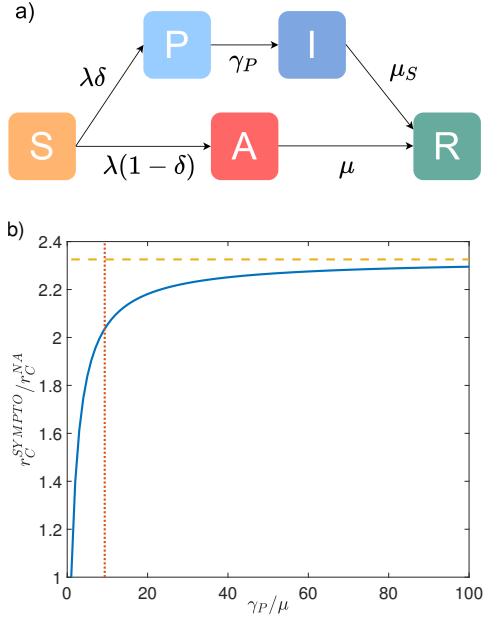


FIG. 1: **Epidemic model without CT.** In panel (a) we represent, the compartmental epidemic model without CT. In panel (b) we plot, as a function of  $\gamma_P/\mu$ , the ratio between the epidemic threshold  $r_C^{SYMPTO}$  when symptomatic nodes are isolated and the epidemic threshold of the non-adaptive case  $r_C^{NA}$ . The horizontal dashed orange line indicates the value of  $r_C^{SYMPTO}/r_C^{NA}$  for  $\gamma_P = \infty$  (instantaneous onset of symptoms). The vertical red dash-dotted line indicates the value of  $\gamma_P/\mu$  we consider in the rest of the paper. We set  $\rho(a_S, b_S) = \rho_S(a_S)\delta(b_S - a_S)$ . The curve does not depend on the specific form of  $\rho_S(a_S)$ .

with rate  $\mu_I = \mu\gamma_P/(\gamma_P - \mu)$ , so that the average infectious period for both symptomatic and asymptomatic is  $\tau$ . We neglect states of hospitalization and exposure and consider recovery without death: this choice does not affect the infection dynamics.

Adaptive behavior of populations exposed to epidemics can be modelled within the activity-driven network framework: infected nodes experience a reduction in activity, due to isolation or the appearance of symptoms; similarly, other individuals undertake self-protective behavior to reduce the probability of contact with an infected node, and this is modelled as a reduction in the attractiveness of infected nodes [41–43]. We assume that symptomatic infected nodes  $I$  are immediately isolated ( $a_I, b_I$ ) = (0, 0), therefore not being able to infect anymore. On the contrary, we assume that recovered  $R$ , asymptomatic  $A$  and presymptomatic  $P$  individuals behave as when they were susceptible ( $a_A, b_A$ ) = ( $a_P, b_P$ ) = ( $a_R, b_R$ ) = ( $a_S, b_S$ ). The adaptive behavior is implemented without affecting the activity of nodes which are not isolated [42].

The control parameter  $r = \lambda/\mu$  is the effective infection rate, whose critical value  $r_C$  – the epidemic threshold – sets the transition point between the absorbing and the active phase of the epidemic. The increase in the value of

$r_C$  is an indicator of the effectiveness of mitigation strategies. Within the adaptive activity-driven framework, the epidemic threshold can be calculated analytically via a mean-field approach (see Materials and Methods).

The effect of isolating symptomatic nodes as the only containment measure is shown in Fig. 1(b). We compare the epidemic threshold  $r_C$ , obtained with the isolation of symptomatic nodes only, with the epidemic threshold  $r_C^{NA}$  of the non-adaptive (NA) case, in which no containment measures are taken on infected individuals, as a function of  $\gamma_P/\mu$  (see Materials and Methods for the explicit expression). In the case of instantaneous symptoms development ( $\gamma_P/\mu \rightarrow \infty$ ), the threshold is increased by a factor of  $1/(1 - \delta)$ , while for smaller  $\gamma_P/\mu$  the gain is reduced. For example, for  $(1 - \delta) = 0.43$ , that is 43% of asymptomatic individuals,  $\tau_P = 1.5$  days and  $\tau = 14$  days as observed for SARS-CoV-2 (see Materials and Methods for details on the parameters used in all figures), the threshold is doubled by the isolation of symptomatic nodes. This is the baseline reference for the evaluation of the performance of CT strategies.

## B. Manual and digital contact tracing protocols

The CT protocols differ in their practical implementation as well in their exploration properties.

### 1. Manual CT

Manual tracing is performed by personnel who, through interviews, collects information, contacts individuals who may have been infected and arranges for testing. In manual CT, as soon as an individual develops symptoms (i.e.  $P \rightarrow I$ ), her contacts in the previous  $T_{CT}$  days are traced with recall probability  $\varepsilon(a)$ , where  $a$  is the activity of the symptomatic individual. A traced contact is tested and, if found in state  $A$  (infected asymptomatic), isolated ( $a = b = 0$ ): the average time between the isolation of the symptomatic individual and the isolation of her asymptomatic infected contacts is  $\tau_C$ . Such delay can be quite large, due to the time required for the collection of the diary, the execution of the diagnostic test and the subsequent isolation [2, 17]. Moreover, the manual protocol depends on  $\varepsilon(a)$ , which takes into account the limited resources allocated for tracing and the limited memory/knowledge of symptomatic individuals in reconstructing their contacts. Low activity nodes make few contacts over time and a fraction of their contacts will be traced; on the other hand high activity nodes will only remember a finite number of their contacts so that, also because of limitations of the tracing capacity, we expect that at most a number  $k_c$  of contacts can be traced [44, 45]. This translates into the limited scalability property:

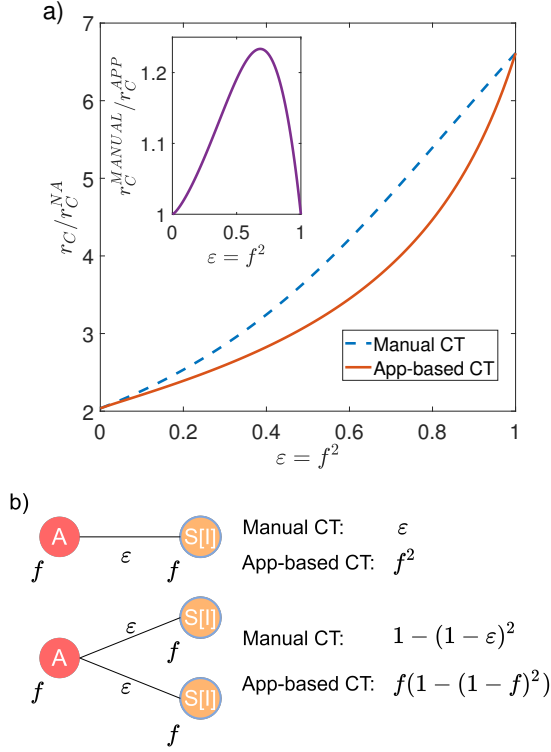


FIG. 2: **Stochastic vs. prearranged sampling in CT.** In panel (a) we plot, as a function of  $\varepsilon = f^2$ , the ratio between the epidemic threshold  $r_C$  in the presence of CT protocols and the epidemic threshold of the non-adaptive case  $r_C^{NA}$ . In the inset we plot the ratio between the epidemic threshold of the manual CT  $r_C^{MANUAL}$  and that of the app-based CT  $r_C^{APP}$ , as a function of  $\varepsilon = f^2$ . We consider homogeneous activity and attractiveness, setting  $\rho(a_S, b_S) = \delta(a_S - a)\delta(b_S - b)$ . Panel (b) shows that if an asymptomatic node  $A$  infects a single susceptible node  $S$  (which subsequently becomes symptomatic,  $I$ ), the infector is traced with probability  $\varepsilon$  in the manual CT and with probability  $f^2$  in the digital CT. Thus the probability is the same if we impose  $f^2 = \varepsilon$ . However, if an asymptomatic node infects two susceptible nodes (which subsequently become symptomatic), the probability of tracing the infector with the manual protocol is  $1 - (1 - \varepsilon)^2 = 2f^2 - f^4$  (still considering  $\varepsilon = f^2$ ), that is always larger than that of the digital protocol  $f(1 - (1 - f^2)^2) = 2f^2 - f^3$ .

$$\varepsilon(a_S) = \begin{cases} \varepsilon^*, & \text{if } a_S \leq a^* \\ \varepsilon^* \frac{a^*}{a_S} = \frac{k_c}{2T_{CT}a_S}, & \text{if } a_S > a^* \end{cases} \quad (2)$$

where  $a^* = k_c/2T_{CT}\varepsilon^*$ .

## 2. App-based CT

Digital CT is based on the download of an app which allows the tracing of close contacts equipped with the same app. We assume that each of the individuals has

a probability  $f$  to download the app before the epidemic starts. As soon as an individual develops symptoms (i.e.  $P \rightarrow I$ ), if she downloaded the app, her contacts are traced only if they downloaded the app as well. A traced contact is tested and, if found in state  $A$  (infected asymptomatic), is isolated,  $a = b = 0$ . The time passing between the isolation of a symptomatic individual and the isolation of her asymptomatic infected contacts is taken to be 0, thus assuming an idealized scenario of instantaneous notification and isolation. See Materials and Methods for details on the implementation of the CT protocols.

## C. Stochastic vs. prearranged sampling

We first compare the two CT protocols in the case of a population with homogeneous activity and attractiveness,  $\rho(a_S, b_S) = \delta(a_S - a)\delta(b_S - b)$ , without delay even in manual CT, i.e.,  $\tau_C = 0$ . We set  $\varepsilon = f^2$  so that the probability that a single contact is traced in the two protocols is the same. However, it should be emphasized that typical values of  $f^2$  range between 0.01 and 0.1 in many countries [30–32], while  $\varepsilon$  is usually larger ( $\approx 0.5$ ), since typically more than half of contacts occur at home, at work or at school and thus are easily traceable [46]. An exact analytical estimate of the epidemic threshold is obtained through a linear stability analysis around the absorbing state (see Materials and Methods for explicit expressions): in Fig. 2(a) we compare the threshold for manual and app-based CT, compared to the non-adaptive case (NA), for realistic COVID-19 parameters. Both protocols feature the same epidemic threshold when  $\varepsilon = f = 0$  and  $\varepsilon = f = 1$ : indeed the former corresponds to the isolation of symptomatic individuals only, without CT, while the latter limit corresponds to the case in which all contacts are traced. For intermediates values of  $\varepsilon = f^2$ , manual tracing is strongly and surprisingly more effective than digital tracing, as it increases significantly the epidemic threshold, compared to the app-based protocol. Since we are considering no heterogeneity or delays, the difference is due only to sampling effects in the CT dynamics. In practice, in app-based CT the population to be tested is prearranged, based on whether or not the app was downloaded before the outbreak started. On the contrary, manual CT performs a stochastic sampling of the population: the random exploration can potentially reach the entire population, since anyone who has come in contact with a symptomatic node can be traced. The simplest example of the difference in tracing multiple infections processes in the two protocols is illustrated in Fig. 2(b).

## D. Effects of heterogeneous activity

We now consider a heterogeneous activity distribution, as observed in several human systems, and we consider



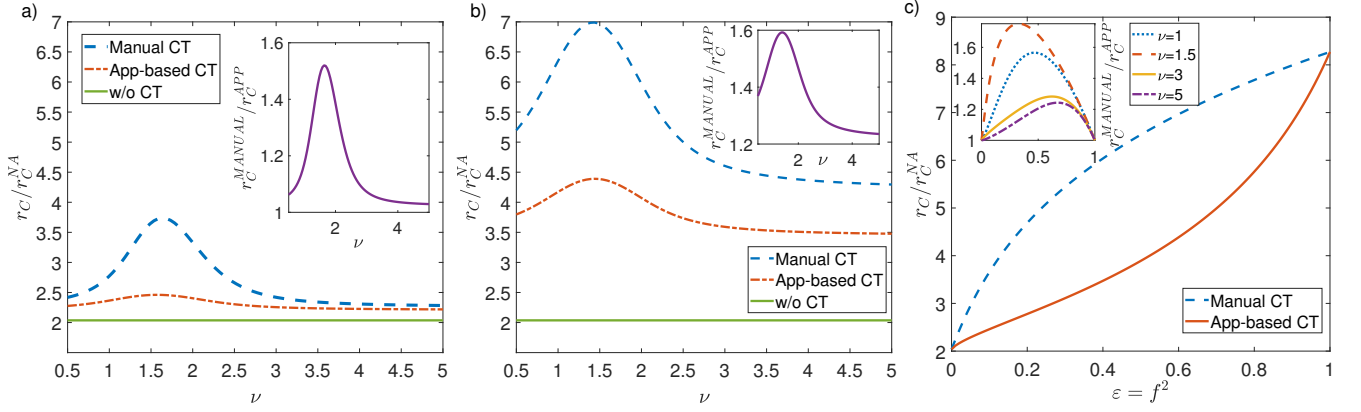


FIG. 3: **Effects of heterogeneity.** In panels (a) and (b) we plot, as a function of the exponent  $\nu$ , the ratio between the epidemic threshold  $r_C$  in the presence of CT protocols and the epidemic threshold of the non-adaptive case  $r_C^{NA}$ . In the inset we plot the ratio between the epidemic threshold of the manual CT  $r_C^{MANUAL}$  and that of the app-based CT  $r_C^{APP}$ , as a function of  $\nu$ . In panel (a)  $\varepsilon = f^2 = 0.1$  ( $f \approx 0.316$ ), in panel (b)  $\varepsilon = f^2 = 0.6$  ( $f \approx 0.775$ ). In panel (c) we plot the ratio  $r_C/r_C^{NA}$  as a function of  $\varepsilon = f^2$  for both CT protocols, with  $\nu = 1.5$ . In the inset we plot the ratio  $r_C^{MANUAL}/r_C^{APP}$  as a function of  $\varepsilon = f^2$  for several  $\nu$  values. In all panels the distribution  $\rho_S(a_S, b_S)$  is given by Eq. (1).

a positive activity-attractiveness correlation, as defined in Eq. (1) [33–37]. The power-law distribution for the activity implies the presence of hubs with high activity and high attractiveness. We investigate the pure effect of heterogeneities in contact tracing [12, 27] setting now  $\varepsilon(a_S) = \varepsilon$ ,  $\forall a_S$  and not considering delays in manual CT,  $\tau_C = 0$ . We perform again a mean-field approach, obtaining an analytical closed form for the epidemic threshold (see Materials and Methods and Supplementary Information, SI): in Fig. 3 we compare the epidemic threshold with the two protocols as a function of the exponent  $\nu$  of the activity distribution, for realistic parameters and setting an average activity  $\bar{a}_S = 6.7 \text{ days}^{-1}$  [41, 46]. Both protocols are more effective in heterogeneous populations  $\nu \sim 1 - 1.5$ . However heterogeneity greatly amplifies stochastic effects, further increasing the advantage of the manual tracing over the app-based prearranged protocol. Indeed, in heterogeneous populations nodes with high activity and attractiveness (super-spreaders) drive and sustain the spread of the epidemic. Manual CT is far more effective in identifying and isolating them than app-based CT: in digital CT, hubs which have not downloaded the app will never be traced, despite the high number of their contacts. On the contrary, manual CT is very effective in tracing super-spreaders, because they are engaged in many contacts and are traced very effectively by stochastic exploration.

#### E. Limited scalability and delay in manual contact tracing

We now consider some features of manual CT that can reduce its effectiveness: the limited scalability of the tracing capacity [44, 45] and the delays in CT and isolation [2, 23, 28]. We set  $\varepsilon(a_S)$  as in Eq. (2) and consider

a large delay  $\tau_C = 3$  days [2] in manual CT. In Fig. 4 we compare the epidemic threshold for the two CT protocols, setting equal the probabilities of tracing a contact  $\bar{\varepsilon} = f^2$ , where  $\bar{\varepsilon} = \int \varepsilon(a_S) \rho_S(a_S)$ . For small values of  $\bar{\varepsilon}$  (note that this however corresponds to a quite large adoption rate  $f = \sqrt{\bar{\varepsilon}} \approx 0.316$ ) manual CT is still more effective (see Fig. 4(a)): the delay in isolation and the limited scalability are not able to significantly reduce the advantage provided by the stochastic exploration of contacts. Fig. 4(b) shows that digital CT can become more effective than manual CT, but this occurs only for very large values of  $f^2$  and  $\tau_C$ . This indicates that for realistic settings, the advantage of the manual protocol over the app-based protocol is robust even including delays and limited scalability. Fig. 4(c) further illustrates for which (unrealistically large) values of  $f^2$  and  $\tau_C$ , digital CT outperforms manual CT. Note that realistic values of  $f$  correspond to  $f^2$  at most of the order of 0.1. Hence, an extremely high adoption of the app is necessary in order to obtain an effective advantage of the digital CT.

#### F. Effects of manual and app-based CT in the epidemic phase

We now explore with numerical simulations (see Materials and Methods, SI) the effects of the CT protocols in the active phase of the epidemic. We consider an optimistic value of  $f = 0.316$ , setting  $\bar{\varepsilon} = f^2 = 0.1$  that is a very low value for the recall probability, and we consider the system above the epidemic threshold  $r > r_C$ , in the conditions of Fig. 4(a). Fig. 5 shows that the infection peak with manual tracing is lower than the app-based one. Moreover, in the manual CT the duration of the epidemic is reduced: this strongly impacts on the final epidemic size, which is about half of the one observed in

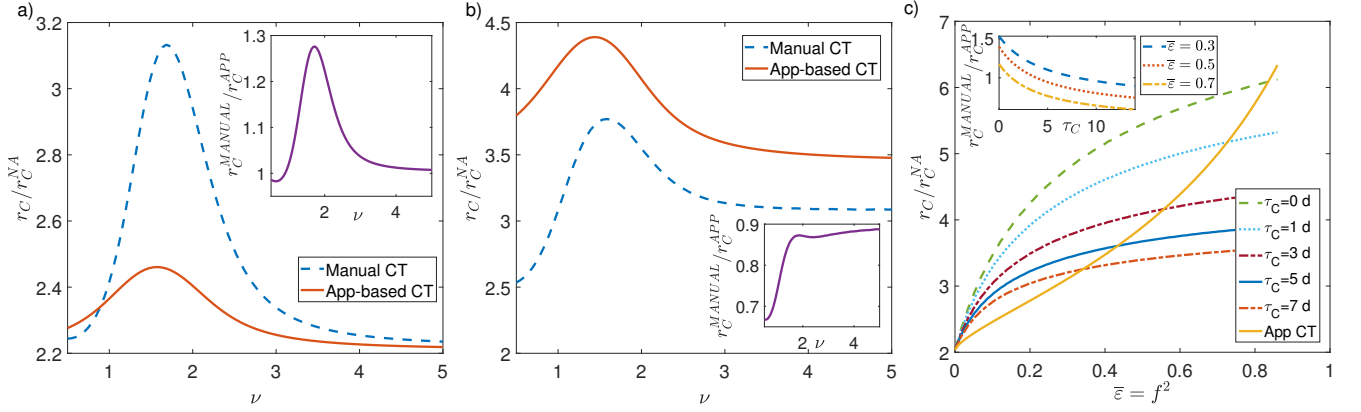


FIG. 4: **Effects of limited scalability and isolation delay in manual CT.** In panels (a) and (b) we plot, as a function of the exponent  $\nu$ , the ratio between the epidemic threshold  $r_C$  in the presence of CT protocols and the epidemic threshold of the non-adaptive case  $r_C^{NA}$ , with limited scalability and delay in manual CT. In the insets we plot the ratio between the epidemic threshold of the manual CT  $r_C^{MANUAL}$  and that of the app-based CT  $r_C^{APP}$ , as a function of  $\nu$ . In panel (a)  $\bar{\epsilon} = f^2 = 0.1$  ( $f \approx 0.316$ ),  $\tau_C = 3$  days, while in panel (b)  $\bar{\epsilon} = f^2 = 0.6$  ( $f \approx 0.775$ ),  $\tau_C = 5$  days. In panel (c) we plot the ratio  $r_C/r_C^{NA}$  as a function of  $\bar{\epsilon} = f^2$  for both CT protocols, setting  $\nu = 1.5$  and for several values of  $\tau_C$ : in the inset we plot the ratio  $r_C^{MANUAL}/r_C^{APP}$  as a function of  $\tau_C$  for several  $\bar{\epsilon}$  values. In all panels the distribution  $\rho_S(a_S, b_S)$  is given by Eq. (1).

the app-based CT. We also plot the temporal evolution of the average activity of the system  $\langle a(t) \rangle$  and of the fraction of isolated nodes  $Iso(t)$  (see inset). In general, the average activity  $\langle a(t) \rangle$  features a minimum, however its value remains very large (about 98% of the case without any tracing measure). This implies that both protocols do not disrupt the functionality of the system. Interestingly, the fraction of isolated nodes is coherent with the infection peak, and in particular it is lower when the infection peak is lowered. This means that the most effective procedure, i.e. manual CT for realistic values of the parameters, not only lowers the infection peak but it is also able to isolate a smaller number of nodes, a key feature of any effective CT strategy.

### G. Robustness

In the SI we show that the advantage of the manual CT is robust with respect to the relaxation of many assumptions and to the change of parameters. In particular, we consider the case where all nodes have equal attractiveness  $\rho(a_S, b_S) = \rho_S(a_S)\delta(b_S - b)$ , we take into account very strong delays  $\tau_C$  and we change the maximum number of traceable contacts  $k_c$ .

## II. DISCUSSION AND CONCLUSIONS

Our results indicate that manual CT, despite its drawbacks, can be an efficient protocol in heterogeneous populations, more efficient than its digital counterpart, due to its specific sampling properties. This conclusion is robust with respect to variations in several model assumptions, including correlations between activity and

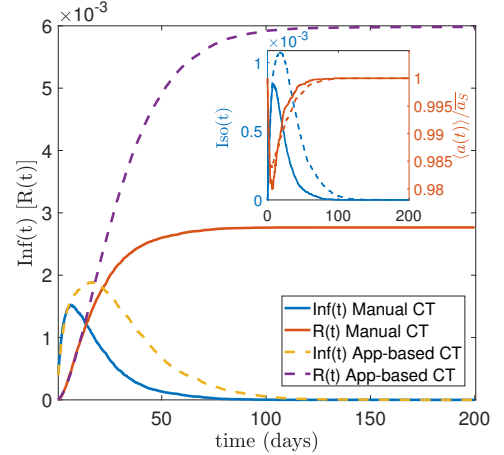


FIG. 5: **Effects of manual and digital CT on the epidemic active phase.** We plot the temporal evolution of the fraction of infected nodes  $Inf(t)$ , i.e. infected asymptomatic and infected symptomatic, and of the fraction of removed nodes  $R(t)$ , for both manual and digital CT. In the inset we plot the temporal evolution of the fraction of isolated nodes  $Iso(t)$  (right y-axis) and of the average activity of the population  $\langle a(t) \rangle$  (left y-axis), normalized with  $\bar{a}_S$ . All curves are averaged on several realizations of the disorder and of the temporal evolution. We set  $\bar{\epsilon} = f^2 = 0.1$ ,  $\tau_C = 3$  days,  $r/r_C^{NA} = 3.1$  and  $N = 5 \cdot 10^3$ . The distribution  $\rho(a_S, b_S)$  is given by Eq. (1), with  $\nu = 1.5$ .

attractiveness or the limited scalability of the manual CT protocol. However, epidemic propagation and strategies to mitigate it are very complex processes and several of their features have been left out from our modelling scheme. Many of them can be included straightforwardly, at the price only of more complicated equations, that can still be solved numerically. Some of these features

(the possibility that isolation is non complete, that some individuals do not report symptoms or the existence of testing campaigns detecting infected nonsymptomatic individuals) act similarly on both types of CT and hence do not modify the relative performance. Other more realistic features (the presence of delays even in digital CT and the existence of additional sources of heterogeneity in viral shedding [47], recovery rates [48] and activity temporal patterns [49]) would even reduce the relative performance of digital CT.

Some effects neglected in the present analysis may in principle improve the performance of digital versus manual CT. In particular, a positive correlation between activity  $a_S$  and probability  $f$  of adopting the app would positively influence the effectiveness of digital CT. This is highly desirable and therefore should be pursued in campaigns to drive app adoption. In general economic, social and psychological factors may affect the choice to use the app, so this represents a challenge for policy makers. Another effect that could enhance CT protocols is following chains of transmissions along multiple steps. In fact in present protocols when a traced contact is found infected also her contacts are often reconstructed and tested. This additional step improves the overall effectiveness of CT protocols, but also increases the delay associated to the manual procedure with respect to the digital one. Digital CT allows in principle to extend very easily the tracing procedure to an arbitrary number of steps, thus enhancing the ability to mitigate the spreading process. However, strong concerns, related to privacy issues [50], make this path difficult to follow.

In summary, additional features in digital CT should be proposed to counterbalance its intrinsic weakness, originated by the nature of the sampling of contacts performed and worsened by unavoidable heterogeneities in the epidemic spreading. This weakness can reduce the effectiveness of the digital CT procedure, even for adoption rates much higher than the values currently observed. The manual CT protocol, with its higher intrinsic stochasticity, does not suffer from this problem and samples contacts effectively, especially in realistic heterogeneous populations: thus, digital CT cannot be considered simply as a cheaper and more rapid way of implementing standard contact tracing. Manual CT must necessarily play an important role in any strategy to mitigate the current pandemic. Considerations about costs and practical feasibility of the two approaches (which have not been taken into account here) suggest that a careful integration of the two protocols may be the key for more effective mitigation strategies. In this respect, the availability of detailed data about the rates of app adoption in various population groups (and correlations with age or activity levels), as well as more precise estimates of other parameters, such as the recall probability, would be highly beneficial. The design of optimal hybrid (manual and digital) CT protocols, including decisions on how to allocate resources and how to target recommendations for app adoption, is a very promising direction for future

work.

### III. MATERIALS AND METHODS

#### A. Mean-field equations and implementation of CT protocols

We consider an activity-attractiveness based mean-field approach, dividing the population into classes of nodes with the same activity  $a_S$  and attractiveness  $b_S$  and treating them as if they were statistically equivalent. For each class  $(a_S, b_S)$  we consider the probability that at time  $t$  a node is in one of the epidemic compartments. For arbitrary  $\rho(a_S, b_S)$  distribution and arbitrary functional form of  $f(a_S)$  and  $\varepsilon(a_S)$  we build the mean-field equations which describe the temporal evolution of the network, the epidemic spreading and the adaptive behavior due to isolation and CT (see SI). In particular, in order to model the manual and app-based CT we introduce two further compartments:  $T$  traceable asymptomatic and  $Q$  isolated asymptomatic. An asymptomatic individual became traceable  $T$  when infected by a presymptomatic node or when she infects a susceptible node that eventually develops symptoms. In the manual case the tracing is effective with probability  $\varepsilon(a)$ . In the app-based case, tracing occurs only if both nodes involved in the contact downloaded the app. A traceable node is still infective  $(a_T, b_T) = (a_S, b_S)$  and with rate  $\gamma_A = 1/\tau_A \gg \mu$  it is quarantined,  $T \xrightarrow{\gamma_A} Q$ ; while a quarantined node is no more infective since  $(a_Q, b_Q) = (0, 0)$ . In order to take into account the delay in the manual CT we set:  $\tau_A = \tau_C + \tau_P$  for the manual case and  $\tau_A = \tau_P$  for the app-based process.

#### B. Epidemic thresholds

We perform a linear stability analysis of the mean field equations around the absorbing state obtaining the conditions for its stability and then the epidemic threshold  $r_C$  (see SI for details). For the non-adaptive case (NA), when infected individuals do not modify their behavior, the threshold is equal to the one obtained in Refs. [35, 42]. Indeed, setting  $\rho(a_S, b_S) = \rho_S(a_S)\delta(b_S - a_S)$  we obtain:

$$r_C^{NA} = \frac{\overline{a_S}}{2a_S^2} \quad (3)$$

If only symptomatic nodes are isolated as soon as they develop symptoms, we obtain, setting  $\rho(a_S, b_S) = \rho_S(a_S)\delta(b_S - a_S)$ :

$$r_C^{SYMPTO} = r_C^{NA} \frac{\frac{\gamma_P}{\mu}}{\delta + (1 - \delta)\frac{\gamma_P}{\mu}} \quad (4)$$

For the case with CT on homogeneous population, we set  $\rho(a_S, b_S) = \delta(a_S - a)\delta(b_S - b)$ ,  $\varepsilon(a_S) = \varepsilon$  and no delay

in manual CT  $\tau_C = 0$ . We obtain the epidemic threshold

for both the manual and digital CT:

$$r_C^{MANUAL} = \frac{2r_C^{NA} \frac{\gamma_P}{\mu}}{\delta + (1 - \delta - \varepsilon\delta) \frac{\gamma_P}{\mu} + \sqrt{(\delta + (1 - \delta - \varepsilon\delta) \frac{\gamma_P}{\mu})^2 + 4\delta^2 \varepsilon \frac{\gamma_P}{\mu}}} \quad (5)$$

$$r_C^{APP} = \frac{2r_C^{NA} \frac{\gamma_P}{\mu}}{\delta + (1 - \delta - f\delta) \frac{\gamma_P}{\mu} + \sqrt{(\delta + (1 - \delta - f\delta) \frac{\gamma_P}{\mu})^2 + 4\delta f \frac{\gamma_P}{\mu} (\delta + \frac{\gamma_P}{\mu} (1 - f)(1 - \delta))}} \quad (6)$$

The more general case of populations with arbitrary distribution  $\rho(a_S, b_S)$ , arbitrary delays  $\tau_C$  and general form of  $\varepsilon(a_S)$  and  $f(a_S)$ , is reported in the SI.

### C. Model parameters

Figures present results where one of the model parameters is varied and all the others are fixed. Here we report the parameter values used throughout the paper, unless specified otherwise. They are tailored to describe the current COVID-19 pandemic.

The fraction of infected individuals who develop symptoms is  $\delta = 0.57$  [1]. The time after which a presymptomatic individual spontaneously develops symptoms is  $\tau_P = 1.5$  days [6, 39, 51], while infected individuals recover on average after  $\tau = 14$  days [40, 47]. The time window over which contacts are reconstructed is  $T_{CT} = 14$  days [51]: it is fixed equal to  $\tau$  to track both nodes infected by the index case in the pre-symptomatic phase (forward CT) and the primary case who infected the index case (backward CT) [12]. The maximum number of contacts engaged in  $T_{CT}$  by a single individual that can be reconstructed with the manual CT procedure is  $k_C = 130$ , according to the estimates of allocated resources [44, 52] and assuming that for an average individual ( $a_S = \bar{a}_S$ ) at most 70% of its contacts

can be traced, since more than half of physical contacts occur at home, at work and at school [46, 51]. The activity-driven network parameters are fixed so that the average value of the activity is always the same, i.e.  $\bar{a}_S = 6.7 \text{ days}^{-1}$  [41, 46]. In particular for a power-law distribution  $\rho_S(a_S) \sim a_S^{-(\nu+1)}$ , the values of  $a_S$  are constrained between a minimum and a maximum value ( $a_m < a_S < a_M$ ). We keep  $a_M = 10^3 a_m$  and then we tune  $a_m$  to set  $\bar{a}_S$ .

### D. Numerical simulations

We perform numerical simulations of the epidemic model on the adaptive activity-driven network: the network dynamics and epidemic spreading are implemented by a continuous time Gillespie-like algorithm. We consider an activity-driven network of  $N$  nodes. The results are averaged over several realizations of the disorder and of the dynamical evolution, so that the error on the infection peak height is lower than 6%. The initial conditions are imposed by infecting the node with the highest activity  $a_S$  and the CT protocols are immediately adopted. A detailed description of the simulations is reported in the SI.

- 
- [1] E. Lavezzo *et al.*, *Nature* **584**, 425 (2020).
  - [2] L. Ferretti *et al.*, *Science* **368**, eabb6936 (2020).
  - [3] C. Rothe *et al.*, *New England Journal of Medicine* **382**, 970 (2020).
  - [4] F. Pinotti *et al.*, *PLOS Medicine* **17**, 1 (2020).
  - [5] R. Li *et al.*, *Science* **368**, 489 (2020).
  - [6] W. E. Wei *et al.*, *Morbidity and Mortality Weekly Report* **69**, 411 (2020).
  - [7] G. Bonaccorsi *et al.*, *Proceedings of the National Academy of Sciences* **117**, 15530 (2020).
  - [8] M. Nicola *et al.*, *International Journal of Surgery* **78**, 185 (2020).
  - [9] K. T. Eames and M. J. Keeling, *Proceedings of the Royal*

- Society of London. Series B: Biological Sciences* **270**, 2565 (2003).
- [10] C. Fraser, S. Riley, R. M. Anderson, and N. M. Ferguson, *Proceedings of the National Academy of Sciences* **101**, 6146 (2004).
- [11] D. Klöckner, C. Fraser, and H. Heesterbeek, *PLOS ONE* **1**, 1 (2006).
- [12] S. Kojaku, L. Hébert-Dufresne, E. Mones, S. Lehmann, and Y.-Y. Ahn, “The effectiveness of contact tracing in heterogeneous networks,” (2020), [arXiv:2005.02362 \[q-bio.PE\]](https://arxiv.org/abs/2005.02362).
- [13] E. McLean *et al.*, *Epidemiology & Infection* **138**, 1531 (2010).



- [14] P. Crook *et al.*, *Emerging infectious diseases* **23**, 2081 (2017).
- [15] D. M. Bell, W. H. O. W. G. on International, and C. T. of SARS, *Emerging infectious diseases* **10**, 1900 (2004).
- [16] A. Wilder-Smith, C. J. Chiew, and V. J. Lee, *The Lancet Infectious Diseases* **20**, e102 (2020).
- [17] J. Hellewell *et al.*, *The Lancet Global Health* **8**, e488 (2020).
- [18] “Privacy-preserving contact tracing,” <https://covid19.apple.com/contacttracing> (2020).
- [19] C. Troncoso *et al.*, “Decentralized privacy-preserving proximity tracing,” (2020), [arXiv:2005.12273 \[cs.CR\]](https://arxiv.org/abs/2005.12273) .
- [20] N. Oliver *et al.*, *Science Advances* **6**, eabc0764 (2020).
- [21] N. Ahmed *et al.*, *IEEE Access* **8**, 134577–134601 (2020).
- [22] P. Sapiezynski, J. Pruessing, and V. Sekara, “The fallibility of contact-tracing apps,” (2020), [arXiv:2005.11297 \[cs.CY\]](https://arxiv.org/abs/2005.11297) .
- [23] I. Braithwaite, T. Callender, M. Bullock, and R. W. Aldridge, *The Lancet Digital Health* (2020).
- [24] M. Zastrow, *Nature* (2020), Technology Feature, 2020-05-19.
- [25] G. Cencetti *et al.*, “Digital proximity tracing in the covid-19 pandemic on empirical contact networks” (2020), [medRxiv:2020.05.29.20115915](https://medrxiv.org/content/2020.05.29.20115915) .
- [26] J. Almagor and S. Picascia, “Can the app contain the spread? an agent-based model of covid-19 and the effectiveness of smartphone-based contact tracing,” (2020), [arXiv:2008.07336 \[cs.CY\]](https://arxiv.org/abs/2008.07336) .
- [27] B. F. Nielsen, K. Sneppen, L. Simonsen, and J. Mathiesen, “Social network heterogeneity is essential for contact tracing,” (2020), [medRxiv:2020.06.05.20123141](https://medrxiv.org/content/2020.06.05.20123141) .
- [28] M. E. Kretzschmar *et al.*, *The Lancet Public Health* **5**, e452 (2020).
- [29] A. Barrat, C. Cattuto, M. Kivelä, S. Lehmann, and J. Saramäki, “Effect of manual and digital contact tracing on covid-19 outbreaks: a study on empirical contact data,” (2020), [medRxiv:2020.07.24.20159947](https://medrxiv.org/content/2020.07.24.20159947) .
- [30] L. Alessandro, *Sole24Ore* (2020), 2020-09-09.
- [31] P. H. O’Neill, Ryan-Mosley, and B. Johnson, *MIT Technology Review* (2020), Tech policy/Privacy, 2020-05-07.
- [32] MIT Technology Review, “Covid tracing tracker,” (2020), accessed on: 2020-09-29.
- [33] N. Perra, B. Gonçalves, R. Pastor-Satorras, and A. Vespignani, *Scientific Reports* **2**, 469 (2012).
- [34] E. Ubaldi *et al.*, *Scientific Reports* **6**, 35724 (2016).
- [35] I. Pozzana, K. Sun, and N. Perra, *Phys. Rev. E* **96**, 042310 (2017).
- [36] E. Ubaldi, A. Vezzani, M. Karsai, N. Perra, and R. Burioni, *Scientific Reports* **7**, 46225 (2017).
- [37] M. Starnini, A. Baronchelli, and R. Pastor-Satorras, *Phys. Rev. Lett.* **110**, 168701 (2013).
- [38] W. Guan *et al.*, *New England Journal of Medicine* **382**, 1708 (2020).
- [39] L. Di Domenico, G. Pullano, C. E. Sabbatini, P.-Y. Boëlle, and V. Colizza, *BMC Medicine* **18**, 240 (2020).
- [40] World Health Organization, *Report of the WHO-China Joint Mission on Coronavirus Disease 2019 (COVID-19)* (2020), accessed on: 2020-09-29.
- [41] K. Van Kerckhove, N. Hens, W. J. Edmunds, and K. T. D. Eames, *American Journal of Epidemiology* **178**, 1655 (2013).
- [42] M. Mancastropa, R. Burioni, V. Colizza, and A. Vezzani, *Phys. Rev. E* **102**, 020301 (2020).
- [43] E. P. Fenichel *et al.*, *Proceedings of the National Academy of Sciences* **108**, 6306 (2011).
- [44] European Center for Disease Prevention and Control, “Resource estimation for contact tracing, quarantine and monitoring activities for covid-19 cases in the eu/eea,” (2020), 2020-03-02.
- [45] Centers for Disease Control and Prevention, “Scaling up staffing roles in case investigation and contact tracing,” (2020), accessed on: 2020-09-29.
- [46] J. Mossong *et al.*, *PLOS Medicine* **5**, 1 (2008).
- [47] Y. Liu *et al.*, *The Lancet Infectious Diseases* **20**, 656 (2020).
- [48] G. F. de Arruda, G. Petri, F. A. Rodrigues, and Y. Moreno, *Phys. Rev. Research* **2**, 013046 (2020).
- [49] M. Mancastropa, A. Vezzani, M. A. Muñoz, and R. Burioni, *Journal of Statistical Mechanics: Theory and Experiment* **2019**, 053502 (2019).
- [50] J. A. Firth *et al.*, *Nature Medicine* (2020).
- [51] M. J. Keeling, T. D. Hollingsworth, and J. M. Read, *Journal of Epidemiology & Community Health* **74**, 861 (2020).
- [52] European Center for Disease Prevention and Control, “Contact tracing for covid-19: current evidence, options for scale-up and an assessment of resources needed,” (2020), 2020-04.

# Supplemental Information for "Stochastic sampling effects favor manual over digital contact tracing"

Marco Mancastropa,<sup>1,2</sup> Claudio Castellano,<sup>3</sup> Alessandro Vezzani,<sup>4,1</sup> and Raffaella Burioni<sup>1,2</sup>

<sup>1</sup>*Dipartimento di Scienze Matematiche, Fisiche e Informatiche,  
Università degli Studi di Parma, Parco Area delle Scienze, 7/A 43124 Parma, Italy*

<sup>2</sup>*INFN, Sezione di Milano Bicocca, Gruppo Collegato di Parma,  
Parco Area delle Scienze, 7/A 43124 Parma, Italy*

<sup>3</sup>*Istituto dei Sistemi Complessi (ISC-CNR), Via dei Taurini 19, I-00185 Roma, Italy*

<sup>4</sup>*Istituto dei Materiali per l'Elettronica ed il Magnetismo (IMEM-CNR),  
Parco Area delle Scienze, 37/A-43124 Parma, Italy*

(Dated: November 17, 2021)

In this supplemental information we derive the mean-field equations for the temporal evolution of the epidemic model on adaptive activity-driven networks. We also derive analytically the epidemic threshold and we describe a scheme of the continuous-time Gillespie-like algorithm used for the numerical approach to the temporal evolution of the network and of the epidemic. Finally, we discuss in detail the robustness of the results.

## I. MEAN-FIELD EQUATIONS AND ANALYTICAL DERIVATION OF THE EPIDEMIC THRESHOLDS

We consider the epidemic model proposed in the main text evolving on an adaptive activity-driven network in the presence of contact tracing of asymptomatic nodes.

The epidemic model proposed is a Susceptible-Infected-Recovered (SIR) model, with a further distinction for the states of infection  $I$ . The distinction is based on the presence of symptoms, on tracing and isolation and it models changes in social behaviour depending on nodes' health status. We do not consider here burstiness effects [1] nor memory [2]. The model is an exact mean-field since local correlations are continuously destroyed due to link reshuffling: thus the epidemic threshold of the  $SIR$  and  $SIS$  epidemic models are the same [2]. Therefore, to obtain the epidemic threshold we consider the mean-field equations for the  $SIS$  version of the model, in which the recovered nodes become susceptible again without gaining immunity.

### A. Manual CT

We now focus on the manual CT and we apply an *activity-attractiveness based mean-field* approach, dividing the population in classes of nodes with same  $(a_S, b_S)$  and considering them statistically equivalent. We assigne initially to each node the status of symptomatic (with probability  $\delta$ ) or asymptomatic (with probability  $1 - \delta$ ), instead of assigning it at the time of infection. This choice is completely equivalent to the epidemic model described and allows us to write the mean-field equations in a simpler way. Thus, at the mean-field level, the epidemic dynamics is described by the probabilities:

- $P_{a_S, b_S}(t)$  for a symptomatic node to be infected pre-symptomatic at time  $t$ ;
- $I_{a_S, b_S}(t)$  for a symptomatic node to be infected symptomatic at time  $t$ ;
- $1 - I_{a_S, b_S}(t) - P_{a_S, b_S}(t)$  to be susceptible at time  $t$ , for a node which will develop symptoms;
- $A_{a_S, b_S}(t)$  for an asymptomatic node to be infected asymptomatic at time  $t$ ;
- $T_{a_S, b_S}(t)$  for an asymptomatic node to be infected traceable at time  $t$ ;
- $Q_{a_S, b_S}(t)$  for an asymptomatic node to be infected isolated at time  $t$ ;
- $1 - A_{a_S, b_S}(t) - Q_{a_S, b_S}(t) - T_{a_S, b_S}(t)$  to be susceptible at time  $t$ , for a node which will not develop symptoms.

In this case the average attractiveness at time  $t$  is  $\langle b(t) \rangle = \bar{b}_S - (1 - \delta)\bar{b}_S Q(t) - \delta\bar{b}_S I(t)$  where we define in general  $\bar{g} = \int da_S db_S \rho(a_S, b_S) g_{a_S, b_S}$ . We consider the system in the thermodynamic limit. The probabilities previously introduced evolve accordingly to the following equations:

$$\begin{aligned} \partial_t P_{a_S, b_S}(t) = & -\gamma_P P_{a_S, b_S}(t) + \lambda a_S(1 - I_{a_S, b_S}(t) - P_{a_S, b_S}(t)) \frac{\delta \overline{b_S P}(t) + (1 - \delta) [\overline{b_S T}(t) + \overline{b_S A}(t)]}{\overline{b_S} - (1 - \delta) \overline{b_S Q}(t) - \delta \overline{b_S I}(t)} \\ & + \lambda b_S(1 - I_{a_S, b_S}(t) - P_{a_S, b_S}(t)) \frac{\delta \overline{a_S P}(t) + (1 - \delta) [\overline{a_S T}(t) + \overline{a_S A}(t)]}{\overline{b_S} - (1 - \delta) \overline{b_S Q}(t) - \delta \overline{b_S I}(t)} \end{aligned} \quad (1)$$

where the first term on right hand side accounts for symptoms onset; the second and third terms account for contagion processes of a susceptible node who engages a contact with a pre-symptomatic or a non-isolated asymptomatic infected node, respectively for the activation of the susceptible and of the infected node. Both terms are averaged over all the activity-attractiveness classes of the infected node.

$$\partial_t I_{a_S, b_S}(t) = -\mu_I I_{a_S, b_S}(t) + \gamma_P P_{a_S, b_S}(t) \quad (2)$$

where the first term on the right hand side accounts for spontaneous recovery and the second term for spontaneous symptoms development.

$$\begin{aligned} \partial_t A_{a_S, b_S}(t) = & -\mu A_{a_S, b_S}(t) + \lambda a_S(1 - A_{a_S, b_S}(t) - T_{a_S, b_S}(t) - Q_{a_S, b_S}(t)) \frac{\delta [\overline{b_S P}(t) - \varepsilon \overline{b_S P}(t)] + (1 - \delta) [\overline{b_S T}(t) + \overline{b_S A}(t)]}{\overline{b_S} - (1 - \delta) \overline{b_S Q}(t) - \delta \overline{b_S I}(t)} \\ & + \lambda b_S(1 - A_{a_S, b_S}(t) - T_{a_S, b_S}(t) - Q_{a_S, b_S}(t)) \frac{\delta [\overline{a_S P}(t) - \varepsilon \overline{a_S P}(t)] + (1 - \delta) [\overline{a_S T}(t) + \overline{a_S A}(t)]}{\overline{b_S} - (1 - \delta) \overline{b_S Q}(t) - \delta \overline{b_S I}(t)} \\ & - \lambda a_S \delta A_{a_S, b_S}(t) \frac{\overline{\varepsilon b_S} - \varepsilon \overline{b_S I}(t) - \varepsilon \overline{b_S P}(t)}{\overline{b_S} - (1 - \delta) \overline{b_S Q}(t) - \delta \overline{b_S I}(t)} - \lambda b_S \delta A_{a_S, b_S}(t) \frac{\overline{\varepsilon a_S} - \varepsilon \overline{a_S I}(t) - \varepsilon \overline{a_S P}(t)}{\overline{b_S} - (1 - \delta) \overline{b_S Q}(t) - \delta \overline{b_S I}(t)} \end{aligned} \quad (3)$$

where the first term on right hand side accounts for spontaneous recovery; the second and third terms account for contagion processes of a susceptible node who engages a contact with a non-isolated asymptomatic infected node or with a pre-symptomatic node and their contact is not traced ( $(1 - \varepsilon(a'_S))$ , with  $a'_S$  activity of the pre-symptomatic node). Both terms are averaged over all the activity-attractiveness classes of the infected node. The fourth and fifth terms correspond to contact tracing of infected asymptomatic due to infection of a susceptible symptomatic and effective CT of the link ( $\varepsilon(a'_S)$ , with  $a'_S$  activity of the pre-symptomatic node). Both terms are averaged over all the activity-attractiveness classes of the susceptible node.

$$\begin{aligned} \partial_t T_{a_S, b_S}(t) = & -(\mu + \gamma_A) T_{a_S, b_S}(t) + \lambda b_S(1 - A_{a_S, b_S}(t) - T_{a_S, b_S}(t) - Q_{a_S, b_S}(t)) \frac{\delta \overline{\varepsilon a_S P}(t)}{\overline{b_S} - (1 - \delta) \overline{b_S Q}(t) - \delta \overline{b_S I}(t)} \\ & + \lambda a_S(1 - A_{a_S, b_S}(t) - T_{a_S, b_S}(t) - Q_{a_S, b_S}(t)) \frac{\delta \overline{\varepsilon b_S P}(t)}{\overline{b_S} - (1 - \delta) \overline{b_S Q}(t) - \delta \overline{b_S I}(t)} \\ & + \lambda b_S \delta A_{a_S, b_S}(t) \frac{\overline{\varepsilon a_S} - \varepsilon \overline{a_S I}(t) - \varepsilon \overline{a_S P}(t)}{\overline{b_S} - (1 - \delta) \overline{b_S Q}(t) - \delta \overline{b_S I}(t)} \\ & + \lambda a_S \delta A_{a_S, b_S}(t) \frac{\overline{\varepsilon b_S} - \varepsilon \overline{b_S I}(t) - \varepsilon \overline{b_S P}(t)}{\overline{b_S} - (1 - \delta) \overline{b_S Q}(t) - \delta \overline{b_S I}(t)} \end{aligned} \quad (4)$$

where the first term on right hand side accounts for isolation and recovery: the rate of isolation is  $\gamma_A = 1/(\tau_C + \tau_P)$ , since a node became traceable  $T$  at time  $t$  in which it engages the traceable link, thus we need to take into account the time for both isolation and symptoms onset. The second and third terms account for contagion processes of a susceptible node who engage a contact with a pre-symptomatic node and their contact is traced ( $\varepsilon(a'_S)$ , with  $a'_S$  activity of the pre-symptomatic node). Both terms are averaged over all the activity-attractiveness classes of the infected node. The fourth and fifth terms correspond to contact tracing of infected asymptomatic due to infection of a susceptible symptomatic and effective CT of the link ( $\varepsilon(a'_S)$ , with  $a'_S$  activity of the pre-symptomatic node). Both terms are averaged over all the activity-attractiveness classes of the susceptible node.

$$\partial_t Q_{a_S, b_S}(t) = -\mu Q_{a_S, b_S}(t) + \gamma_A T_{a_S, b_S}(t) \quad (5)$$

where the first term on right hand side accounts for spontaneous recovery and the second term for isolation of traceable asymptomatic infected nodes.

This set of equations admits as a stationary state the absorbing state, a configuration where all the population is susceptible. To obtain the condition for the stability of the absorbing state, i.e. the epidemic threshold, we apply a linear stability analysis around the absorbing state.

Let us now consider the case of realistic correlations between the activity and attractiveness [3, 4]:  $\rho(a_S, b_S) = \rho_S(a_S)\delta(b_S - a_S)$ , with generic  $\rho_S(a_S)$ . If we average the equations on all activity classes, we obtain the temporal evolution of the average probabilities  $\bar{P}(t)$ ,  $\bar{I}(t)$ ,  $\bar{A}(t)$ ,  $\bar{T}(t)$ ,  $\bar{Q}(t)$ ; similarly we obtain the temporal evolution of  $\overline{a_S T}(t)$ ,  $\overline{a_S A}(t)$ ,  $\overline{a_S P}(t)$  and  $\overline{\varepsilon a_S P}(t)$  multiplying the equations for  $a_S \rho_S(a_S)$  or  $\varepsilon(a_S) a_S \rho_S(a_S)$  and integrating. Neglecting second order terms in probabilities, we obtain a linearized set of 9 differential equations:

$$\partial_t \bar{I}(t) = -\mu_I \bar{I}(t) + \gamma_P \bar{P}(t) \quad (6)$$

$$\partial_t \bar{P}(t) = -\gamma_P \bar{P}(t) + 2\lambda[\delta \overline{a_S P}(t) + (1 - \delta)(\overline{a_S T}(t) + \overline{a_S A}(t))] \quad (7)$$

$$\partial_t \bar{Q}(t) = -\mu \bar{Q}(t) + \gamma_A \bar{T}(t) \quad (8)$$

$$\partial_t \bar{T}(t) = -(\mu + \gamma_A) \bar{T}(t) + 2\lambda \delta \overline{\varepsilon a_S P}(t) + 2\lambda \delta \overline{a_S A}(t) \frac{\overline{\varepsilon a_S}}{\overline{a_S}} \quad (9)$$

$$\partial_t \bar{A}(t) = -\mu \bar{A}(t) + 2\lambda[\delta(\overline{a_S P}(t) - \overline{\varepsilon a_S P}(t)) + (1 - \delta)(\overline{a_S T}(t) + \overline{a_S A}(t))] - 2\lambda \delta \overline{a_S A}(t) \frac{\overline{\varepsilon a_S}}{\overline{a_S}} \quad (10)$$

$$\partial_t \overline{a_S P}(t) = -\gamma_P \overline{a_S P}(t) + 2\lambda \frac{\overline{a_S^2}}{\overline{a_S}} [\delta \overline{a_S P}(t) + (1 - \delta)(\overline{a_S T}(t) + \overline{a_S A}(t))] \quad (11)$$

$$\partial_t \overline{\varepsilon a_S P}(t) = -\gamma_P \overline{\varepsilon a_S P}(t) + 2\lambda \frac{\overline{\varepsilon a_S^2}}{\overline{a_S}} [\delta \overline{a_S P}(t) + (1 - \delta)(\overline{a_S T}(t) + \overline{a_S A}(t))] \quad (12)$$

$$\partial_t \overline{a_S T}(t) = -(\mu + \gamma_A) \overline{a_S T}(t) + 2\lambda \delta \frac{\overline{a_S^2}}{\overline{a_S}} \overline{\varepsilon a_S P}(t) + 2\lambda \delta \overline{a_S A}(t) \frac{\overline{\varepsilon a_S}}{\overline{a_S}} \quad (13)$$

$$\partial_t \overline{a_S A}(t) = -\mu \overline{a_S A}(t) + 2\lambda \frac{\overline{a_S^2}}{\overline{a_S}} [\delta(\overline{a_S P}(t) - \overline{\varepsilon a_S P}(t)) + (1 - \delta)(\overline{a_S T}(t) + \overline{a_S A}(t))] - 2\lambda \delta \overline{a_S A}(t) \frac{\overline{\varepsilon a_S}}{\overline{a_S}} \quad (14)$$

The linearized equations for the dynamic evolution of  $\overline{a_S^n A}(t)$  and  $\overline{a_S^n T}(t)$  always involve terms like  $\overline{a_S^{n+1} A}(t)$ , due to the contact tracing terms. This would produce an infinite set of coupled linear differential equations: to close the equations and obtain a complete set of linearized equations, we express  $\overline{a_S^2 A}(t)$  in terms of the other average probabilities. By definition  $\overline{a_S^2 A}(t) = \int da_S \rho_S(a_S) a_S^2 A_{a_S}(t)$ : since we are interested in studying the absorbing steady state, we consider Eq. (3) for  $\rho(a_S, b_S) = \rho_S(a_S)\delta(b_S - a_S)$ , linearized around the absorbing state and near the stationary condition  $\partial_t A_{a_S}(t) \sim 0$ :

$$A_{a_S}(t) \simeq \frac{2\lambda a_S [\delta(\overline{a_S P}(t) - \overline{\varepsilon a_S P}(t)) + (1 - \delta)(\overline{a_S T}(t) + \overline{a_S A}(t))]}{\mu \overline{a_S} + 2\lambda \delta a_S \overline{\varepsilon a_S}} \quad (15)$$

Thus, setting  $r = \lambda/\mu$  and replacing Eq. (15) into the definition of  $\overline{a_S^2 A}(t)$  we obtain:

$$\overline{a_S^2 A}(t) \simeq \frac{2r}{\overline{a_S}} [\delta(\overline{a_S P}(t) - \overline{\varepsilon a_S P}(t)) + (1 - \delta)(\overline{a_S T}(t) + \overline{a_S A}(t))] K \quad (16)$$

where  $K = \frac{\overline{a_S^3}}{1 + 2r \delta \overline{a_S} \frac{\overline{\varepsilon a_S}}{\overline{a_S}}} = \int da_S \rho_S(a_S) \frac{a_S^3}{1 + 2r \delta a_S \frac{\overline{\varepsilon a_S}}{\overline{a_S}}}$ .

In this way we obtain the following linearized equations for  $\overline{a_S T}(t)$  and  $\overline{a_S A}(t)$ , near the absorbing stationary state:

$$\partial_t \overline{a_S T}(t) = -(\mu + \gamma_A) \overline{a_S T}(t) + 2\lambda \delta \frac{\overline{a_S^2}}{\overline{a_S}} \overline{\varepsilon a_S P}(t) + 4\lambda r \frac{\overline{\varepsilon a_S}}{\overline{a_S^2}} \delta K [\delta(\overline{a_S P}(t) - \overline{\varepsilon a_S P}(t)) + (1 - \delta)(\overline{a_S T}(t) + \overline{a_S A}(t))] \quad (17)$$

$$\begin{aligned} \partial_t \overline{a_S A}(t) = & -\mu \overline{a_S A}(t) + 2\lambda \frac{\overline{a_S^2}}{\overline{a_S}} [\delta(\overline{a_S P}(t) - \overline{\varepsilon a_S P}(t)) + (1 - \delta)(\overline{a_S T}(t) + \overline{a_S A}(t))] \\ & - 4\lambda r \frac{\overline{\varepsilon a_S}}{\overline{a_S^2}} \delta K [\delta(\overline{a_S P}(t) - \overline{\varepsilon a_S P}(t)) + (1 - \delta)(\overline{a_S T}(t) + \overline{a_S A}(t))] \end{aligned} \quad (18)$$

We focus on the Jacobian matrix of this set of 9 linearized equations:

$$J = \begin{bmatrix} -\mu_I & \gamma_P & 0 & 0 & 0 & 0 & 0 & 0 & 0 \\ 0 & -\gamma_P & 0 & 0 & 0 & 2\lambda\delta & 0 & 2\lambda(1-\delta) & 2\lambda(1-\delta) \\ 0 & 0 & -\mu & \gamma_A & 0 & 0 & 0 & 0 & 0 \\ 0 & 0 & 0 & -\mu - \gamma_A & 0 & 0 & 2\lambda\delta & 0 & 2\lambda\delta \frac{\varepsilon a_S}{a_S} \\ 0 & 0 & 0 & 0 & -\mu & 2\lambda\delta & -2\lambda\delta & 2\lambda(1-\delta) & 2\lambda(1-\delta) - 2\lambda\delta \frac{\varepsilon a_S}{a_S} \\ 0 & 0 & 0 & 0 & 0 & -\gamma_P + \Delta & 0 & \Gamma & \Gamma \\ 0 & 0 & 0 & 0 & 0 & \phi & -\gamma_P & \Phi & \Phi \\ 0 & 0 & 0 & 0 & 0 & \theta & \Delta - \theta & -\mu - \gamma_A + \Psi & \Psi \\ 0 & 0 & 0 & 0 & 0 & \Delta - \theta & \theta - \Delta & \Gamma - \Psi & -\mu + \Gamma - \Psi \end{bmatrix} = \begin{bmatrix} \mathbb{A}(5 \times 5) & \mathbb{C}(5 \times 4) \\ \mathbb{O}(4 \times 5) & \mathbb{B}(4 \times 4) \end{bmatrix} \quad (19)$$

where  $\Delta = 2\lambda\delta \frac{a_S^2}{a_S}$ ,  $\Gamma = 2\lambda(1-\delta) \frac{a_S^2}{a_S}$ ,  $\phi = 2\lambda\delta \frac{\varepsilon a_S^2}{a_S}$ ,  $\Phi = 2\lambda(1-\delta) \frac{\varepsilon a_S^2}{a_S}$ ,  $\theta = 4\lambda r \delta^2 \frac{\varepsilon a_S}{a_S^2} K$  and  $\Psi = 4\lambda r \delta(1-\delta) \frac{\varepsilon a_S}{a_S^2} K$ .

The Jacobian matrix is a block matrix and the condition for the stability of the absorbing state is obtained imposing all eigenvalues to be negative. We can consider separately the two blocks on the diagonal: for the first block  $\mathbb{A}$  it is evident that the eigenvalues are  $\xi_{1,2} = -\mu$ ,  $\xi_3 = -\mu_I$ ,  $\xi_4 = -\gamma_P$ ,  $\xi_5 = -\mu - \gamma_A$ , all negative. Therefore, it is sufficient to study block  $\mathbb{B}$ , which is a matrix  $4 \times 4$ . The characteristic polynomial of  $\mathbb{B}$  is a polynomial of degree 4, thus we apply the Descartes' rule of signs to impose all roots to be negative and we obtain the condition for the stability of the absorbing state:

$$8r^3\delta^2(1-\delta) \frac{\varepsilon a_S^2 \varepsilon a_S}{a_S} \frac{a_S^3}{1 + 2r\delta a_S \frac{\varepsilon a_S}{a_S}} \frac{\gamma_A}{\mu} - 4r^2\delta(1-\delta) \left[ \frac{\varepsilon a_S^2 a_S^2}{\mu} + \frac{\gamma_P}{\mu} \frac{\varepsilon a_S}{a_S} \frac{a_S^3}{1 + 2r\delta a_S \frac{\varepsilon a_S}{a_S}} \right] \frac{\gamma_A}{\mu} + 2ra_S^2 \frac{\gamma_A}{\mu} \left( \frac{\gamma_A}{\mu} + 1 \right) \left( \delta + \frac{\gamma_P}{\mu} (1-\delta) \right) - \frac{\gamma_P}{\mu} \left( \frac{\gamma_A}{\mu} + 1 \right) < 0 \quad (20)$$

By setting the equality, the equation allows to obtain a closed relation for estimating the epidemic threshold  $r_C$ . The epidemic threshold obtained with the mean-field approach is exact and it holds for manual contact tracing, with arbitrary delay  $\tau_C$  (encapsulated in  $\gamma_A$ ), for arbitrary  $\rho_S(a_S)$  and  $\varepsilon(a_S)$ .

## B. App-based CT

Analogously we apply the *activity-attractiveness based mean-field* approach to the app-based CT. At the mean-field level, the epidemic dynamics is described by the probabilities:

- $P_{a_S, b_S}(t)$  for a symptomatic node without app to be infected pre-symptomatic at time  $t$ ;
- $I_{a_S, b_S}(t)$  for a symptomatic node without app to be infected symptomatic at time  $t$ ;
- $1 - P_{a_S, b_S}(t) - I_{a_S, b_S}(t)$  to be susceptible at time  $t$ , for a node without app and which will develop symptoms;
- $A_{a_S, b_S}(t)$  for an asymptomatic node without app to be infected asymptomatic at time  $t$ ;
- $1 - A_{a_S, b_S}(t)$  to be susceptible at time  $t$ , for a node without app and which will not develop symptoms;
- $P_{a_S, b_S}^\alpha(t)$  for a symptomatic node with app to be infected pre-symptomatic at time  $t$ ;
- $I_{a_S, b_S}^\alpha(t)$  for a symptomatic node with app to be infected symptomatic at time  $t$ ;
- $1 - P_{a_S, b_S}^\alpha(t) - I_{a_S, b_S}^\alpha(t)$  to be susceptible at time  $t$ , for a node with app and which will develop symptoms;
- $A_{a_S, b_S}^\alpha(t)$  for an asymptomatic node with app to be infected asymptomatic at time  $t$ ;
- $T_{a_S, b_S}^\alpha(t)$  for an asymptomatic node with app to be infected traceable at time  $t$ ;
- $Q_{a_S, b_S}^\alpha(t)$  for an asymptomatic node with app to be infected isolated at time  $t$ ;
- $1 - A_{a_S, b_S}^\alpha(t) - Q_{a_S, b_S}^\alpha(t) - T_{a_S, b_S}^\alpha(t)$  to be susceptible at time  $t$ , for a node with app and which will not develop symptoms.



In this case the average attractiveness at time  $t$  is  $\langle b(t) \rangle = \overline{b_S} - (1 - \delta)\overline{fb_S Q^\alpha(t)} - \delta\overline{fb_S I^\alpha(t)} + \overline{(1 - f)b_S I(t)}$ . We consider the system in the thermodynamic limit: the probabilities previously introduced evolve according to the following equations, obtained analogously to those for manual CT:

$$\partial_t I_{a_S, b_S}(t) = -\mu I_{a_S, b_S}(t) + \gamma_P P_{a_S, b_S}(t) \quad (21)$$

$$\begin{aligned} \partial_t P_{a_S, b_S}(t) = & -\gamma_P P_{a_S, b_S}(t) \\ & + \lambda a_S(1 - I_{a_S, b_S}(t) - P_{a_S, b_S}(t)) \frac{\delta(\overline{fb_S P^\alpha(t)} + \overline{(1 - f)b_S P(t)}) + (1 - \delta)(\overline{fb_S T^\alpha(t)} + \overline{fb_S A^\alpha(t)} + \overline{(1 - f)b_S A(t)})}{\overline{b_S} - (1 - \delta)\overline{fb_S Q^\alpha(t)} - \delta(\overline{fb_S I^\alpha(t)} + \overline{(1 - f)b_S I(t)})} \\ & + \lambda b_S(1 - I_{a_S, b_S}(t) - P_{a_S, b_S}(t)) \frac{\delta(\overline{fa_S P^\alpha(t)} + \overline{(1 - f)a_S P(t)}) + (1 - \delta)(\overline{fa_S T^\alpha(t)} + \overline{fa_S A^\alpha(t)} + \overline{(1 - f)a_S A(t)})}{\overline{b_S} - (1 - \delta)\overline{fb_S Q^\alpha(t)} - \delta(\overline{fb_S I^\alpha(t)} + \overline{(1 - f)b_S I(t)})} \end{aligned} \quad (22)$$

$$\partial_t I_{a_S, b_S}^\alpha(t) = -\mu I_{a_S, b_S}^\alpha(t) + \gamma_P P_{a_S, b_S}^\alpha(t) \quad (23)$$

$$\begin{aligned} \partial_t P_{a_S, b_S}^\alpha(t) = & -\gamma_P P_{a_S, b_S}^\alpha(t) \\ & + \lambda a_S(1 - I_{a_S, b_S}^\alpha(t) - P_{a_S, b_S}^\alpha(t)) \frac{\delta(\overline{fb_S P^\alpha(t)} + \overline{(1 - f)b_S P(t)}) + (1 - \delta)(\overline{fb_S T^\alpha(t)} + \overline{fb_S A^\alpha(t)} + \overline{(1 - f)b_S A(t)})}{\overline{b_S} - (1 - \delta)\overline{fb_S Q^\alpha(t)} - \delta(\overline{fb_S I^\alpha(t)} + \overline{(1 - f)b_S I(t)})} \\ & + \lambda b_S(1 - I_{a_S, b_S}^\alpha(t) - P_{a_S, b_S}^\alpha(t)) \frac{\delta(\overline{fa_S P^\alpha(t)} + \overline{(1 - f)a_S P(t)}) + (1 - \delta)(\overline{fa_S T^\alpha(t)} + \overline{fa_S A^\alpha(t)} + \overline{(1 - f)a_S A(t)})}{\overline{b_S} - (1 - \delta)\overline{fb_S Q^\alpha(t)} - \delta(\overline{fb_S I^\alpha(t)} + \overline{(1 - f)b_S I(t)})} \end{aligned} \quad (24)$$

$$\partial_t A_{a_S, b_S}(t) = -\mu A_{a_S, b_S}(t) \quad (25)$$

$$\begin{aligned} & + \lambda a_S(1 - A_{a_S, b_S}(t)) \frac{\delta(\overline{fb_S P^\alpha(t)} + \overline{(1 - f)b_S P(t)}) + (1 - \delta)(\overline{fb_S T^\alpha(t)} + \overline{fb_S A^\alpha(t)} + \overline{(1 - f)b_S A(t)})}{\overline{b_S} - (1 - \delta)\overline{fb_S Q^\alpha(t)} - \delta(\overline{fb_S I^\alpha(t)} + \overline{(1 - f)b_S I(t)})} \\ & + \lambda b_S(1 - A_{a_S, b_S}(t)) \frac{\delta(\overline{fa_S P^\alpha(t)} + \overline{(1 - f)a_S P(t)}) + (1 - \delta)(\overline{fa_S T^\alpha(t)} + \overline{fa_S A^\alpha(t)} + \overline{(1 - f)a_S A(t)})}{\overline{b_S} - (1 - \delta)\overline{fb_S Q^\alpha(t)} - \delta(\overline{fb_S I^\alpha(t)} + \overline{(1 - f)b_S I(t)})} \end{aligned}$$

$$\begin{aligned} \partial_t A_{a_S, b_S}^\alpha(t) = & -\mu A_{a_S, b_S}^\alpha(t) \\ & + \lambda a_S(1 - A_{a_S, b_S}^\alpha(t) - T_{a_S, b_S}^\alpha(t) - Q_{a_S, b_S}^\alpha(t)) \frac{\delta(\overline{(1 - f)b_S P(t)} + (1 - \delta)(\overline{fb_S T^\alpha(t)} + \overline{fb_S A^\alpha(t)} + \overline{(1 - f)b_S A(t)}))}{\overline{b_S} - (1 - \delta)\overline{fb_S Q^\alpha(t)} - \delta(\overline{fb_S I^\alpha(t)} + \overline{(1 - f)b_S I(t)})} \\ & + \lambda b_S(1 - A_{a_S, b_S}^\alpha(t) - T_{a_S, b_S}^\alpha(t) - Q_{a_S, b_S}^\alpha(t)) \frac{\delta(\overline{(1 - f)a_S P(t)} + (1 - \delta)(\overline{fa_S T^\alpha(t)} + \overline{fa_S A^\alpha(t)} + \overline{(1 - f)a_S A(t)}))}{\overline{b_S} - (1 - \delta)\overline{fb_S Q^\alpha(t)} - \delta(\overline{fb_S I^\alpha(t)} + \overline{(1 - f)b_S I(t)})} \\ & - \lambda \delta a_S A_{a_S, b_S}^\alpha(t) \frac{\overline{fb_S} - \overline{fb_S P^\alpha(t)} - \overline{fb_S I^\alpha(t)}}{\overline{b_S} - (1 - \delta)\overline{fb_S Q^\alpha(t)} - \delta(\overline{fb_S I^\alpha(t)} + \overline{(1 - f)b_S I(t)})} \\ & - \lambda \delta b_S A_{a_S, b_S}^\alpha(t) \frac{\overline{fa_S} - \overline{fa_S P^\alpha(t)} - \overline{fa_S I^\alpha(t)}}{\overline{b_S} - (1 - \delta)\overline{fb_S Q^\alpha(t)} - \delta(\overline{fb_S I^\alpha(t)} + \overline{(1 - f)b_S I(t)})} \end{aligned} \quad (26)$$

$$\partial_t Q_{a_S, b_S}^\alpha(t) = -\mu Q_{a_S, b_S}^\alpha(t) + \gamma_P T_{a_S, b_S}^\alpha(t) \quad (27)$$

$$\partial_t T_{a_S, b_S}^\alpha(t) = -(\mu + \gamma_P) T_{a_S, b_S}^\alpha(t) \quad (28)$$

$$\begin{aligned} & + \lambda a_S(1 - A_{a_S, b_S}^\alpha(t) - T_{a_S, b_S}^\alpha(t) - Q_{a_S, b_S}^\alpha(t)) \frac{\delta \overline{fb_S P^\alpha(t)}}{\overline{b_S} - (1 - \delta)\overline{fb_S Q^\alpha(t)} - \delta(\overline{fb_S I^\alpha(t)} + \overline{(1 - f)b_S I(t)})} \\ & + \lambda b_S(1 - A_{a_S, b_S}^\alpha(t) - T_{a_S, b_S}^\alpha(t) - Q_{a_S, b_S}^\alpha(t)) \frac{\delta \overline{fa_S P^\alpha(t)}}{\overline{b_S} - (1 - \delta)\overline{fb_S Q^\alpha(t)} - \delta(\overline{fb_S I^\alpha(t)} + \overline{(1 - f)b_S I(t)})} \\ & + \lambda \delta a_S A_{a_S, b_S}^\alpha(t) \frac{\overline{fb_S} - \overline{fb_S P^\alpha(t)} - \overline{fb_S I^\alpha(t)}}{\overline{b_S} - (1 - \delta)\overline{fb_S Q^\alpha(t)} - \delta(\overline{fb_S I^\alpha(t)} + \overline{(1 - f)b_S I(t)})} \\ & + \lambda \delta b_S A_{a_S, b_S}^\alpha(t) \frac{\overline{fa_S} - \overline{fa_S P^\alpha(t)} - \overline{fa_S I^\alpha(t)}}{\overline{b_S} - (1 - \delta)\overline{fb_S Q^\alpha(t)} - \delta(\overline{fb_S I^\alpha(t)} + \overline{(1 - f)b_S I(t)})} \end{aligned}$$

This set of equations admits as a stationary state the absorbing state, a configuration where all the population is susceptible. To obtain the condition for the stability of the absorbing state, i.e. the epidemic threshold, we apply a linear stability analysis around the absorbing state.

Let us now consider the case of realistic correlations between the activity and attractiveness:  $\rho(a_S, b_S) = \rho_S(a_S)\delta(b_S - a_S)$ , with general  $\rho(a_S)$ . If we average on all activity classes, we obtain the temporal evolution of the average probabilities  $\overline{P(t)}$ ,  $\overline{I(t)}$ ,  $\overline{A(t)}$ ,  $\overline{P^\alpha(t)}$ ,  $\overline{I^\alpha(t)}$ ,  $\overline{A^\alpha(t)}$ ,  $\overline{Q^\alpha(t)}$ ,  $\overline{T^\alpha(t)}$ ; similarly we obtain the temporal evolution of

$\overline{fa_S P^\alpha}(t)$ ,  $\overline{fa_S T^\alpha}(t)$ ,  $\overline{a_S A^\alpha}(t)$ ,  $\overline{fa_S A^\alpha}(t)$ ,  $\overline{(1-f)a_S P}(t)$ ,  $\overline{(1-f)a_S A}(t)$ , multiplying the equations for  $f(a_S)a_S\rho_S(a_S)$  or  $a_S\rho_S(a_S)$  or  $(1-f(a_S))a_S\rho_S(a_S)$  and integrating over all activity classes. We neglect the terms of second order in probabilities obtaining a linearized set of 14 differential equations:

$$\partial_t \bar{I}(t) = -\mu_I \bar{I}(t) + \gamma_P \bar{P}(t) \quad (29)$$

$$\partial_t \bar{P}(t) = -\gamma_P \bar{P}(t) + 2\lambda[\delta(\overline{fa_S P^\alpha}(t) + \overline{(1-f)a_S P}(t)) + (1-\delta)(\overline{fa_S T^\alpha}(t) + \overline{fa_S A^\alpha}(t) + \overline{(1-f)a_S A}(t))] \quad (30)$$

$$\partial_t \bar{I}^\alpha(t) = -\mu_I \bar{I}^\alpha(t) + \gamma_P \bar{P}^\alpha(t) \quad (31)$$

$$\partial_t \bar{P}^\alpha(t) = -\gamma_P \bar{P}^\alpha(t) + 2\lambda[\delta(\overline{fa_S P^\alpha}(t) + \overline{(1-f)a_S P}(t)) + (1-\delta)(\overline{fa_S T^\alpha}(t) + \overline{fa_S A^\alpha}(t) + \overline{(1-f)a_S A}(t))] \quad (32)$$

$$\partial_t \bar{A}(t) = -\mu \bar{A}(t) + 2\lambda[\delta(\overline{fa_S P^\alpha}(t) + \overline{(1-f)a_S P}(t)) + (1-\delta)(\overline{fa_S T^\alpha}(t) + \overline{fa_S A^\alpha}(t) + \overline{(1-f)a_S A}(t))] \quad (33)$$

$$\partial_t \bar{Q}^\alpha(t) = -\mu \bar{Q}^\alpha(t) + \gamma_P \bar{T}^\alpha(t) \quad (34)$$

$$\partial_t \bar{T}^\alpha(t) = -(\mu + \gamma_P) \bar{T}^\alpha(t) + 2\lambda\delta \overline{fa_S P^\alpha}(t) + 2\lambda\delta \overline{a_S A^\alpha}(t) \frac{\overline{fa_S}}{\overline{a_S}} \quad (35)$$

$$\begin{aligned} \partial_t \bar{A}^\alpha(t) = & -\mu \bar{A}^\alpha(t) + 2\lambda[\delta(\overline{(1-f)a_S P}(t) + (1-\delta)(\overline{fa_S T^\alpha}(t) + \overline{fa_S A^\alpha}(t) + \overline{(1-f)a_S A}(t))] \\ & - 2\lambda\delta \overline{a_S A^\alpha}(t) \frac{\overline{fa_S}}{\overline{a_S}} \end{aligned} \quad (36)$$

$$\begin{aligned} \partial_t \overline{a_S A^\alpha}(t) = & -\mu \overline{a_S A^\alpha}(t) + 2\lambda \frac{\overline{a_S^2}}{\overline{a_S}} [\delta(\overline{(1-f)a_S P}(t) + (1-\delta)(\overline{fa_S T^\alpha}(t) + \overline{fa_S A^\alpha}(t) + \overline{(1-f)a_S A}(t))] \\ & - 2\lambda\delta \overline{a_S^2 A^\alpha}(t) \frac{\overline{fa_S}}{\overline{a_S}} \end{aligned} \quad (37)$$

$$\begin{aligned} \partial_t \overline{fa_S P^\alpha}(t) = & -\gamma_P \overline{fa_S P^\alpha}(t) \\ & + 2\lambda \frac{\overline{fa_S^2}}{\overline{a_S}} [\delta(\overline{fa_S P^\alpha}(t) + \overline{(1-f)a_S P}(t)) + (1-\delta)(\overline{fa_S T^\alpha}(t) + \overline{fa_S A^\alpha}(t) + \overline{(1-f)a_S A}(t))] \end{aligned} \quad (38)$$

$$\begin{aligned} \partial_t \overline{(1-f)a_S P}(t) = & -\gamma_P \overline{(1-f)a_S P}(t) \\ & + 2\lambda \frac{\overline{(1-f)a_S^2}}{\overline{a_S}} [\delta(\overline{fa_S P^\alpha}(t) + \overline{(1-f)a_S P}(t)) + (1-\delta)(\overline{fa_S T^\alpha}(t) + \overline{fa_S A^\alpha}(t) + \overline{(1-f)a_S A}(t))] \end{aligned} \quad (39)$$

$$\begin{aligned} \partial_t \overline{(1-f)a_S A}(t) = & -\mu \overline{(1-f)a_S A}(t) \\ & + 2\lambda \frac{\overline{(1-f)a_S^2}}{\overline{a_S}} [\delta(\overline{fa_S P^\alpha}(t) + \overline{(1-f)a_S P}(t)) + (1-\delta)(\overline{fa_S T^\alpha}(t) + \overline{fa_S A^\alpha}(t) + \overline{(1-f)a_S A}(t))] \end{aligned} \quad (40)$$

$$\partial_t \overline{fa_S T^\alpha}(t) = -(\mu + \gamma_P) \overline{fa_S T^\alpha}(t) + 2\lambda\delta \frac{\overline{fa_S^2}}{\overline{a_S}} \overline{fa_S P^\alpha}(t) + 2\lambda\delta \overline{fa_S^2 A^\alpha}(t) \frac{\overline{fa_S}}{\overline{a_S}} \quad (41)$$

$$\begin{aligned} \partial_t \overline{fa_S A^\alpha}(t) = & -\mu \overline{fa_S A^\alpha}(t) + 2\lambda \frac{\overline{fa_S^2}}{\overline{a_S}} [\delta(\overline{(1-f)a_S P}(t) + (1-\delta)(\overline{fa_S T^\alpha}(t) + \overline{fa_S A^\alpha}(t) + \overline{(1-f)a_S A}(t))] \\ & - 2\lambda\delta \overline{fa_S^2 A^\alpha}(t) \frac{\overline{fa_S}}{\overline{a_S}} \end{aligned} \quad (42)$$

Similarly to the manual CT, in order to close the equations and obtain a complete set of linearized equations, we express  $\overline{fa_S^2 A^\alpha}(t)$  and  $\overline{a_S^2 A^\alpha}(t)$  in terms of the other average probabilities using their own definition. By definition  $\overline{fa_S^2 A^\alpha}(t) = \int da_S \rho_S(a_S) f(a_S) a_S^2 A_{a_S}^\alpha(t)$  and  $\overline{a_S^2 A^\alpha}(t) = \int da_S \rho_S(a_S) a_S^2 A_{a_S}^\alpha(t)$ : since we are interested in studying the steady state and its stability, we consider the Eq. (26) for  $\rho(a_S, b_S) = \rho_S(a_S) \delta(b_S - a_S)$ , linearized around the absorbing state and near to the stationary condition  $\partial_t A_{a_S}^\alpha(t) \sim 0$ :

$$A_{a_S}^\alpha(t) \simeq \frac{2\lambda a_S [\delta(\overline{(1-f)a_S P}(t) + (1-\delta)(\overline{fa_S T^\alpha}(t) + \overline{fa_S A^\alpha}(t) + \overline{(1-f)a_S A}(t))]}{\mu \overline{a_S} + 2\lambda \delta \overline{a_S} \overline{fa_S}} \quad (43)$$

Thus,

$$\overline{fa_S^2 A^\alpha}(t) \simeq \frac{2}{\overline{a_S}} r [\delta(\overline{(1-f)a_S P}(t) + (1-\delta)(\overline{fa_S T^\alpha}(t) + \overline{fa_S A^\alpha}(t) + \overline{(1-f)a_S A}(t))] H \quad (44)$$

$$\overline{a_S^2 A^\alpha}(t) \simeq \frac{2}{\overline{a_S}} r [\delta(\overline{(1-f)a_S P}(t) + (1-\delta)(\overline{fa_S T^\alpha}(t) + \overline{fa_S A^\alpha}(t) + \overline{(1-f)a_S A}(t))] Z \quad (45)$$

where  $H = \frac{\overline{fa_S^3}}{1+2r\delta a_S \frac{\overline{fa_S}}{a_S}} = \int da_S \rho_S(a_S) \frac{f(a_S)a_S^3}{1+2r\delta a_S \frac{\overline{fa_S}}{a_S}}$ ,  $Z = \frac{\overline{a_S^3}}{1+2r\delta a_S \frac{\overline{fa_S}}{a_S}}$ .

In this way we obtain the following linearized equations for  $\overline{fa_S T^\alpha}$ ,  $\overline{fa_S A^\alpha}$  and  $\overline{a_S A^\alpha}$  near the absorbing stationary state:

$$\partial_t \overline{a_S A^\alpha}(t) = -\mu \overline{a_S A^\alpha}(t) + 2\lambda \frac{\overline{a_S^2}}{a_S} [\delta(1-f) \overline{a_S P}(t) + (1-\delta)(\overline{fa_S T^\alpha}(t) + \overline{fa_S A^\alpha}(t) + \overline{(1-f)a_S A}(t))] \quad (46)$$

$$- 4\lambda r \delta \frac{\overline{fa_S}}{a_S^2} [\delta(1-f) \overline{a_S P}(t) + (1-\delta)(\overline{fa_S T^\alpha}(t) + \overline{fa_S A^\alpha}(t) + \overline{(1-f)a_S A}(t))] Z$$

$$\partial_t \overline{fa_S T^\alpha}(t) = -(\mu + \gamma_P) \overline{fa_S T^\alpha}(t) + 2\lambda \delta \frac{\overline{fa_S^2}}{a_S} \overline{fa_S P^\alpha}(t) \quad (47)$$

$$+ 4\lambda r \delta \frac{\overline{fa_S}}{a_S^2} [\delta(1-f) \overline{a_S P}(t) + (1-\delta)(\overline{fa_S T^\alpha}(t) + \overline{fa_S A^\alpha}(t) + \overline{(1-f)a_S A}(t))] H$$

$$\partial_t \overline{fa_S A^\alpha}(t) = -\mu \overline{fa_S A^\alpha}(t) + 2\lambda \frac{\overline{fa_S^2}}{a_S} [\delta(1-f) \overline{a_S P}(t) + (1-\delta)(\overline{fa_S T^\alpha}(t) + \overline{fa_S A^\alpha}(t) + \overline{(1-f)a_S A}(t))] \quad (48)$$

$$- 4\lambda r \delta \frac{\overline{fa_S}}{a_S^2} [\delta(1-f) \overline{a_S P}(t) + (1-\delta)(\overline{fa_S T^\alpha}(t) + \overline{fa_S A^\alpha}(t) + \overline{(1-f)a_S A}(t))] H$$

Focusing on the Jacobian matrix of this set of 14 linearized equations:

$$J = \begin{bmatrix} -\mu_I & \gamma_P & 0 & 0 & 0 & 0 & 0 & 0 & 0 & 0 & 0 & 0 & 0 & 0 \\ 0 & -\gamma_P & 0 & 0 & 0 & 0 & 0 & 0 & 0 & 2\lambda\delta & 2\lambda\delta & 2\lambda(1-\delta) & 2\lambda(1-\delta) & 2\lambda(1-\delta) \\ 0 & 0 & -\mu_I & \gamma_P & 0 & 0 & 0 & 0 & 0 & 0 & 0 & 0 & 0 & 0 \\ 0 & 0 & 0 & -\gamma_P & 0 & 0 & 0 & 0 & 0 & 2\lambda\delta & 2\lambda\delta & 2\lambda(1-\delta) & 2\lambda(1-\delta) & 2\lambda(1-\delta) \\ 0 & 0 & 0 & 0 & -\mu & 0 & 0 & 0 & 0 & 2\lambda\delta & 2\lambda\delta & 2\lambda(1-\delta) & 2\lambda(1-\delta) & 2\lambda(1-\delta) \\ 0 & 0 & 0 & 0 & 0 & -\mu & +\gamma_P & 0 & 0 & 0 & 0 & 0 & 0 & 0 \\ 0 & 0 & 0 & 0 & 0 & 0 & -\mu - \gamma_P & 0 & 2\lambda\delta \frac{\overline{fa_S}}{a_S} & 2\lambda\delta & 0 & 0 & 0 & 0 \\ 0 & 0 & 0 & 0 & 0 & 0 & 0 & -\mu & -2\lambda\delta \frac{\overline{fa_S}}{a_S} & 0 & 2\lambda\delta & 2\lambda(1-\delta) & 2\lambda(1-\delta) & 2\lambda(1-\delta) \\ 0 & 0 & 0 & 0 & 0 & 0 & 0 & 0 & -\mu & 0 & \Delta + \phi - \Phi \frac{Z}{H} & \theta + \Gamma - \Psi \frac{Z}{H} & \theta + \Gamma - \Psi \frac{Z}{H} & \theta + \Gamma - \Psi \frac{Z}{H} \\ 0 & 0 & 0 & 0 & 0 & 0 & 0 & 0 & 0 & -\gamma_P + \Delta & \Delta & \Gamma & \Gamma & \Gamma \\ 0 & 0 & 0 & 0 & 0 & 0 & 0 & 0 & 0 & \phi & -\gamma_P + \phi & \theta & \theta & \theta \\ 0 & 0 & 0 & 0 & 0 & 0 & 0 & 0 & 0 & \phi & \phi & -\mu + \theta & \theta & \theta \\ 0 & 0 & 0 & 0 & 0 & 0 & 0 & 0 & 0 & \Delta & \Phi & \Psi & -\mu - \gamma_P + \Psi & \Psi \\ 0 & 0 & 0 & 0 & 0 & 0 & 0 & 0 & 0 & 0 & \Delta - \Phi & \Gamma - \Psi & \Gamma - \Psi & -\mu + \Gamma - \Psi \end{bmatrix}$$

$$= \begin{bmatrix} \mathbb{A}(9 \times 9) & \mathbb{C}(9 \times 5) \\ \mathbb{O}(5 \times 9) & \mathbb{B}(5 \times 5) \end{bmatrix} \quad (49)$$

where  $\Delta = 2\lambda\delta \frac{\overline{fa_S^2}}{a_S}$ ,  $\Gamma = 2\lambda(1-\delta) \frac{\overline{fa_S^2}}{a_S}$ ,  $\phi = 2\lambda\delta \frac{(1-f)\overline{a_S^2}}{a_S}$ ,  $\theta = 2\lambda(1-\delta) \frac{(1-f)\overline{a_S^2}}{a_S}$ ,  $\Phi = 4\lambda r \delta^2 \frac{\overline{fa_S}}{a_S^2} H$  and  $\Psi = 4\lambda r \delta(1-\delta) \frac{\overline{fa_S}}{a_S^2} H$ .

The Jacobian matrix is a block matrix and we can consider separately the two blocks on the diagonal: for the first block  $\mathbb{A}$  it is evident that the eigenvalues are  $\xi_{1,2} = -\mu_I$ ,  $\xi_{3,4,5,6} = -\mu$ ,  $\xi_{7,8} = -\gamma_P$ ,  $\xi_9 = -\mu - \gamma_P$ , all negative. Therefore, it is sufficient to study block  $\mathbb{B}$ , which is a matrix  $5 \times 5$ . The characteristic polynomial of  $\mathbb{B}$  is a polynomial of degree 5: we apply the Descartes' rule of signs, to impose all roots to be negative and we obtain the condition for the stability of the absorbing state:

$$8r^3\delta^2(1-\delta) \frac{\overline{fa_S^2} \overline{fa_S}}{a_S} \frac{\overline{fa_S^3}}{1+2r\delta a_S \frac{\overline{fa_S}}{a_S}} \frac{\gamma_P}{\mu} - 4r^2\delta(1-\delta) \left[ \frac{\overline{fa_S^2}}{a_S} + \frac{\gamma_P}{\mu} \overline{fa_S} \frac{\overline{fa_S^3}}{1+2r\delta a_S \frac{\overline{fa_S}}{a_S}} \right] \frac{\gamma_P}{\mu} \quad (50)$$

$$+ 2r\overline{a_S^2} \overline{a_S} \left( \frac{\gamma_P}{\mu} + 1 \right) \left( \delta + \frac{\gamma_P}{\mu} (1-\delta) \right) - \overline{a_S^2} \frac{\gamma_P}{\mu} \left( \frac{\gamma_P}{\mu} + 1 \right) < 0$$

By setting the equality, the equation allows to obtain a closed relation for an estimate of the epidemic threshold. The epidemic threshold obtained with the mean-field approach is exact and it holds for digital contact tracing, with arbitrary  $\rho_S(a_S)$  and  $f(a_S)$ .

### C. Limit cases

The obtained closed relations for the stability of the absorbing state in the manual and digital CT hold for arbitrary  $\rho_S(a_S)$ , for completely general  $f(a_S)$  and  $\varepsilon(a_S)$  and for general delays: this allows to introduce complicated effects, such as delay in isolation, activity heterogeneities and limited scalability of the system.

Due to the complicated structure of the equations for the stability (Eq. (20) and Eq. (50)), it is possible to derive the epidemic threshold  $r_C$  only by solving the equation numerically. However, there are some simple limit cases in which the equations are considerably simplified, allowing to obtain the epidemic threshold in an explicit analytic form.

#### 1. Non-adaptive case (NA)

Here we consider the non-adaptive case, in which no adaptive behaviour are implemented, i.e. infected nodes behave as if they were susceptible, with  $(a_I, b_I) = (a_S, b_S)$ . Thus, in this case  $f(a_S) = \varepsilon(a_S) = 0$ ,  $\forall a_S$  and  $\gamma_P/\mu = 1$ . Replacing these values either in Eq. (20) or in Eq. (50) we obtain, as expected:

$$2ra_S^2\overline{a_S} - \overline{a_S}^2 = 0$$

So we obtain an explicit form for the epidemic threshold  $r_C$  in the non-adaptive case:

$$r_C^{NA} = \frac{\overline{a_S}}{2a_S^2} \quad (51)$$

which is the Eq. (3) in the main paper. It reproduces the results previously obtained in Refs. [3, 5].

#### 2. Isolation of only symptomatic nodes

Here we consider the case in which only symptomatic nodes are isolated as soon as they develops symptoms, i.e. no CT is implemented. Thus, in this case  $f(a_S) = \varepsilon(a_S) = 0$ ,  $\forall a_S$ , while  $(a_I, b_I) = (0, 0)$ . Replacing these values either in Eq. (20) or in Eq. (50) we obtain, as expected:

$$2ra_S^2\overline{a_S} \left( \delta + (1 - \delta) \frac{\gamma_P}{\mu} \right) - \overline{a_S}^2 \frac{\gamma_P}{\mu} = 0$$

So we obtain an explicit form for the epidemic threshold  $r_C$ :

$$r_C^{SYMPTO} = r_C^{NA} \frac{\frac{\gamma_P}{\mu}}{\delta + (1 - \delta) \frac{\gamma_P}{\mu}} \quad (52)$$

which is the Eq. (4) in the main paper. For instantaneous symptoms development  $\gamma_P/\mu \rightarrow \infty$  it reproduces the results previously obtained in Ref. [5], and for  $\gamma_P/\mu = 1$  it reproduces the NA case (Eq. (51)).

#### 3. Homogeneous case without delays and without limited scalability

Here we consider the case in which the population is homogeneous, i.e.  $\rho(a_S, b_S) = \delta(a_S - a)\delta(b_S - b)$ , with constant probability of downloading the app in digital CT, i.e.  $f(a_S) = f$ , and constant probability for a contact to be traced in manual CT, i.e.  $\varepsilon(a_S) = \varepsilon$ . Moreover we assume  $\tau_C = 0$ , that is  $\gamma_A = \gamma_P$ . Replacing these values in the Eq. (20), for the manual CT we obtain a quadratic equation in  $r$ :

$$4a^2\delta^2\varepsilon r^2 + 2a \left( \delta + \frac{\gamma_P}{\mu} (1 - \delta - \delta\varepsilon) \right) r - \frac{\gamma_P}{\mu} = 0$$

The equation can be solved and we obtain:

$$r_C^{MANUAL} = r_C^{NA} \frac{2 \frac{\gamma_P}{\mu}}{\delta + (1 - \delta - \varepsilon \delta) \frac{\gamma_P}{\mu} + \sqrt{(\delta + (1 - \delta - \varepsilon \delta) \frac{\gamma_P}{\mu})^2 + 4 \delta^2 \varepsilon \frac{\gamma_P}{\mu}}} \quad (53)$$

which is the Eq. (5) in the main paper.

Analogously, replacing the values in the Eq. (50) for the digital CT we obtain an equation of second degree in  $r$ :

$$4a^2 \delta f \left( \delta + \frac{\gamma_P}{\mu} (1 - \delta)(1 - f) \right) r^2 + 2a \left( \delta + \frac{\gamma_P}{\mu} (1 - \delta - \delta f) \right) r - \frac{\gamma_P}{\mu} = 0$$

The equation can be solved and we obtain:

$$r_C^{APP} = r_C^{NA} \frac{2 \frac{\gamma_P}{\mu}}{\delta + (1 - \delta - f \delta) \frac{\gamma_P}{\mu} + \sqrt{(\delta + (1 - \delta - f \delta) \frac{\gamma_P}{\mu})^2 + 4 \delta f \frac{\gamma_P}{\mu} (\delta + \frac{\gamma_P}{\mu} (1 - f)(1 - \delta))}} \quad (54)$$

which is the Eq. (6) in the main paper.

## II. CONTINUOUS TIME GILLESPIE-LIKE ALGORITHM FOR NETWORK DYNAMICS AND EPIDEMIC EVOLUTION

The network dynamics is performed by a continuous-time Gillespie-like algorithm [6]: we assign to each node the activity  $a_S$  and attractiveness  $b_S$  drawn from the joint distribution  $\rho(a_S, b_S)$ . Initially, the network evolves in the absorbing state, i.e. all nodes are susceptible and infection does not propagate, up to a relaxation time  $t_0$ , to reach the equilibrium of activation dynamics:

1. The first activation time,  $t_i$ , of each node  $i$  is drawn from  $\Psi_{a_S^i}(t_i) = a_S^i e^{-a_S^i t_i}$  at time  $t = 0$ .
2. The node  $i$  with the lowest  $t_i$  activates and connects  $m$  randomly-selected nodes, with probability proportional to their attractiveness  $b_S$ .
3. The next activation time  $t_i$  for node  $i$  is set to  $t_i + \tau$ , with  $\tau$  inter-event time drawn from  $\Psi_{a_S^i}(\tau)$ .
4. All links are destroyed and the process is iterated from point 2.

Then we start the epidemic and contact tracing dynamics as follows:

1. At time  $t = t_0$  the population is divided into a configuration of susceptible ( $S$ ) and infected ( $P$  or  $A$ ) nodes, moreover each node has an activation time  $t_i > t_0 = t$  obtained from the initial relaxation dynamics.
2. Node  $i$  with the lowest  $t_i$  activates. Asymptomatic ( $A$ ,  $T$  and  $Q$ ) and symptomatic nodes ( $I$ ) at time  $t$  recover at  $t_i$  with probability respectively  $1 - e^{-\mu(t_i - t)}$  and  $1 - e^{-\mu_I(t_i - t)}$ : recovered nodes change their activity and attractiveness into  $(a_R, b_R) = (a_S, b_S)$ . Traceable nodes at time  $t$  are isolated at  $t_i$  with probability  $1 - e^{-(t_i - t)/\tau_C}$  (with  $\tau_C > 0$  for manual CT and  $\tau_C = 0$  for digital CT) and set their activity and attractiveness to zero  $(a_Q, b_Q) = (0, 0)$ .
3. Pre-symptomatic nodes at time  $t$  develop symptoms at  $t_i$  with probability  $1 - e^{-\gamma_P(t_i - t)}$ : they set to zero their activity and attractiveness  $(a_I, b_I) = (0, 0)$  and the contact tracing is activated.

**Manual CT:** the protocol is enabled for every symptomatic node. Every contact made in the last  $T_{CT}$  period has  $\varepsilon(a_S)$  probability of being identified and tested, with  $a_S$  activity of the symptomatic node. Every node tested and found infected asymptomatic  $A$  becomes traceable  $T$ .

**Digital CT:** the protocol is enabled only if the symptomatic node has downloaded the app. Each contact made in the last  $T_{CT}$  period with an individual who downloaded the app is identified and tested. Every node tested and found infected asymptomatic  $A$  becomes traceable  $T$ .



4. We set the actual time  $t = t_i$  and the active agent  $i$  generates exactly  $m$  links with  $m$  nodes randomly-chosen with probability proportional to their attractiveness  $b$  at time  $t$  (depending on their status and isolation). The contacts are registered in the contact list of both nodes engaged in the connection. If the link involves a susceptible and an infected node ( $P$ ,  $A$  or  $T$ ), a contagion can occur with probability  $\lambda$  and the susceptible node becomes pre-symptomatic with probability  $\delta$  or asymptomatic with probability  $1 - \delta$ .
5. The new activation time of node  $i$  is  $t_i = t + \tau$  and it is obtained drawing the inter-event time  $\tau$  from the inter-event time distribution  $\Psi_{a^i}(\tau) = a^i e^{-a^i \tau}$ , where  $a^i$  is the activity of node  $i$  at time  $t$ . All the links are deleted and the process is iterated from point 2.

### III. ROBUSTNESS OF THE RESULTS

The advantage of the manual CT is robust relaxing many assumptions and changing most parameters in the modelling scheme.

The results are robust to changes in the maximum number of traceable contacts  $k_c$  in the manual CT: an increase in  $k_c$  reduces the effects of limited scalability; similarly, its reduction makes the effects of limited scalability stronger. However, modifying  $k_c$  with realistic values changes only slightly the epidemic threshold of the manual contact tracing protocol, without changing qualitatively the results, since the manual protocol remains more effective than the digital one, for small  $\bar{\varepsilon} = f^2$  values (Fig. 1(a)).

The results are also robust when considering changes in the social properties of the population, i.e. assuming a different functional form of the  $\rho(a_S, b_S)$  distribution. For example, we can assume that all nodes feature equal attractiveness  $b$  and different activity:  $\rho(a_S, b_S) = \rho_S(a_S)\delta(b_S - b)$ . In this case the correlations between activity and attractiveness are removed: however, again the manual CT is more effective than the digital one in heterogeneous populations and for small  $\bar{\varepsilon} = f^2$  (Fig. 1(b)). The differences between the two methods are reduced, compared to the case with correlations (see the inset of Fig. 1(b)), due to the reduction in heterogeneities, since homogeneous terms are introduced assuming all the nodes having the same attractiveness. However, differences between the two protocols remain evident, even in the presence of delays  $\tau_C > 0$  and limited scalability in the manual CT.

Similarly, the advantage of manual contact tracing holds also considering limited scalability and stronger delays in manual contact tracing  $\tau_C$ : even for a delay of 7 days the manual CT remains more effective than the digital one, for small  $\bar{\varepsilon} = f^2$  and in heterogeneous populations (Fig. 1(c)).

The results are also robust when considering the effects of contact tracing on the active phase of the epidemic: as expected from the analysis on the epidemic threshold, the differences between the two methods are reduced increasing  $\tau_C$ , however even with considerable delays  $\tau_C$  the manual CT for small values of  $\bar{\varepsilon} = f^2$  is more effective in flattening the infection peak and in lowering the epidemic final-size (Fig. 2). Indeed, its effectiveness, compared to the digital CT, is maximized for  $\tau_C = 0$  (Fig. 2(a)); the differences are reduced but still present considering strong delays in manual CT, such as  $\tau_C = 5$  days (Fig. 2(b)). The differences remain even if we consider the system deeply in the active phase, that is for  $r \gg r_C$ : in this case the differences are slightly reduced due to the high infectivity of the system, however again the manual method for small  $\bar{\varepsilon}$  is more effective than digital CT (Fig. 2(c)). Finally, as observed for the epidemic threshold, for very large  $\bar{\varepsilon} = f^2 = 0.6$  and strong delays  $\tau_C = 5$  days, the digital protocol becomes more effective in reducing the impact of the epidemic, further flattening the infection peak and reducing the epidemic final-size (Fig. 2(d)). This again confirms that the effects of the protocols on the active phase are similar to those observed on the epidemic threshold, including the differences in the two approaches.

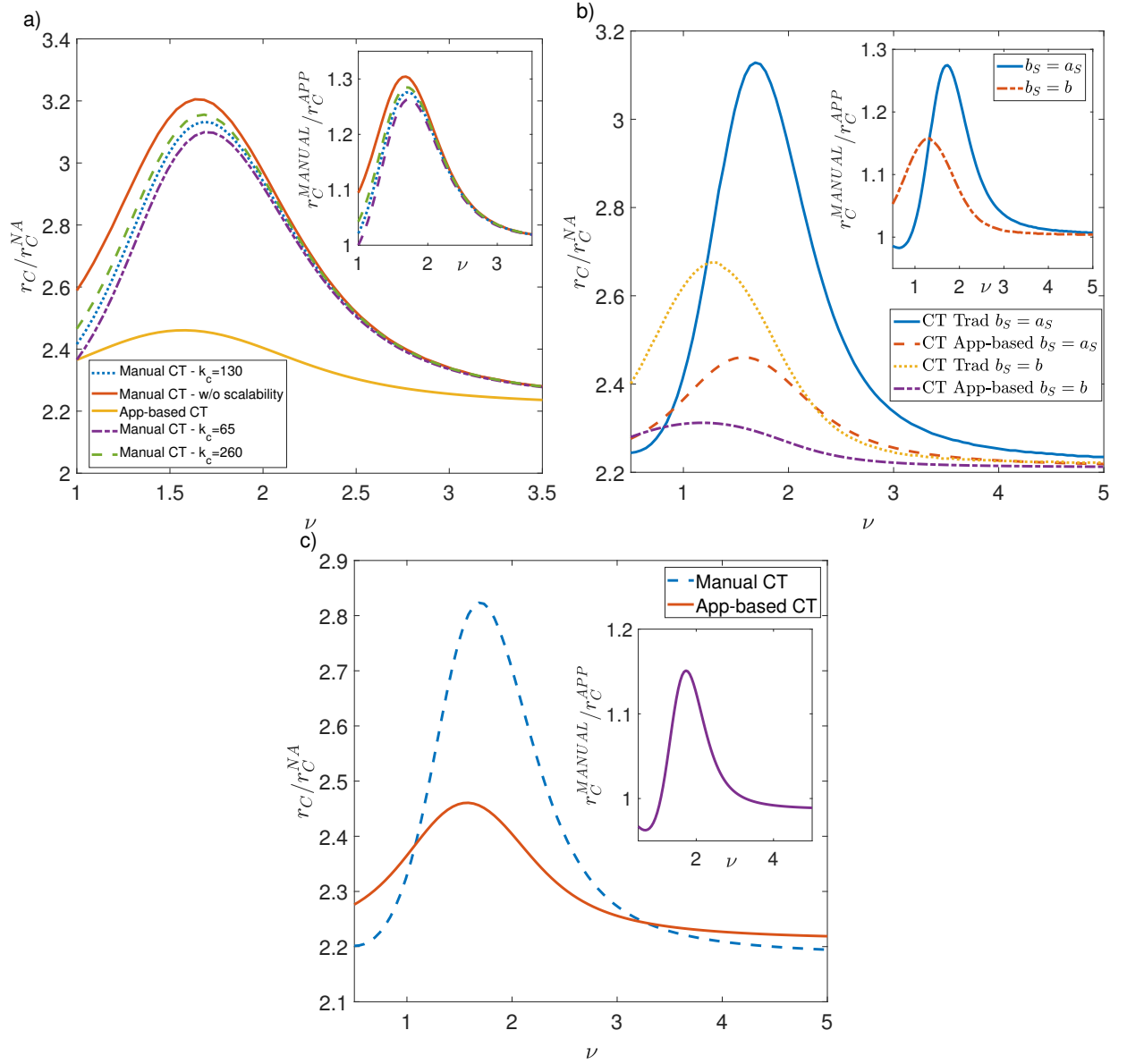


FIG. 1: **Robustness of the results for the epidemic threshold.** In all panels we plot the ratio between the epidemic threshold  $r_C$  in the presence of contact tracing protocols and the epidemic threshold of the non-adaptive case  $r_C^{NA}$ . The ratio is plotted for both manual and digital contact tracing, as a function of  $\nu$ . In all the inserts we plot the ratio between the epidemic threshold of the manual contact tracing  $r_C^{MANUAL}$  and that of the app-based contact tracing  $r_C^{APP}$ , as a function of  $\nu$ . In panel (a) the ratio for the manual CT is plotted for several values of  $k_c$  and also when scalability is not considered (legend), setting  $\tau_C = 3$  days and  $\rho(a_S, b_S) \sim a^{-(\nu+1)}\delta(b_S - a_S)$ . In panel (b) the ratio is plotted both for  $\rho(a_S, b_S) \sim a^{-(\nu+1)}\delta(b_S - a_S)$  and for  $\rho(a_S, b_S) \sim a^{-(\nu+1)}\delta(b_S - b)$  (legend), setting  $\tau_C = 3$  days and  $k_c = 130$ . In panel (c) the ratio is plotted for  $\rho(a_S, b_S) \sim a^{-(\nu+1)}\delta(b_S - a_S)$  setting  $\tau_C = 7$  days and  $k_c = 130$ . In all panels  $\bar{\epsilon} = f^2 = 0.1$ ,  $\nu = 1.5$ ,  $\delta = 0.57$ ,  $\tau_P = 1.5$  days,  $\tau = 14$  days,  $T_{CT} = 14$  days,  $a_S \in [a_M, a_M]$  with  $a_M/a_m = 10^3$ ,  $\bar{a}_S = 6.7 \text{ days}^{-1}$ .

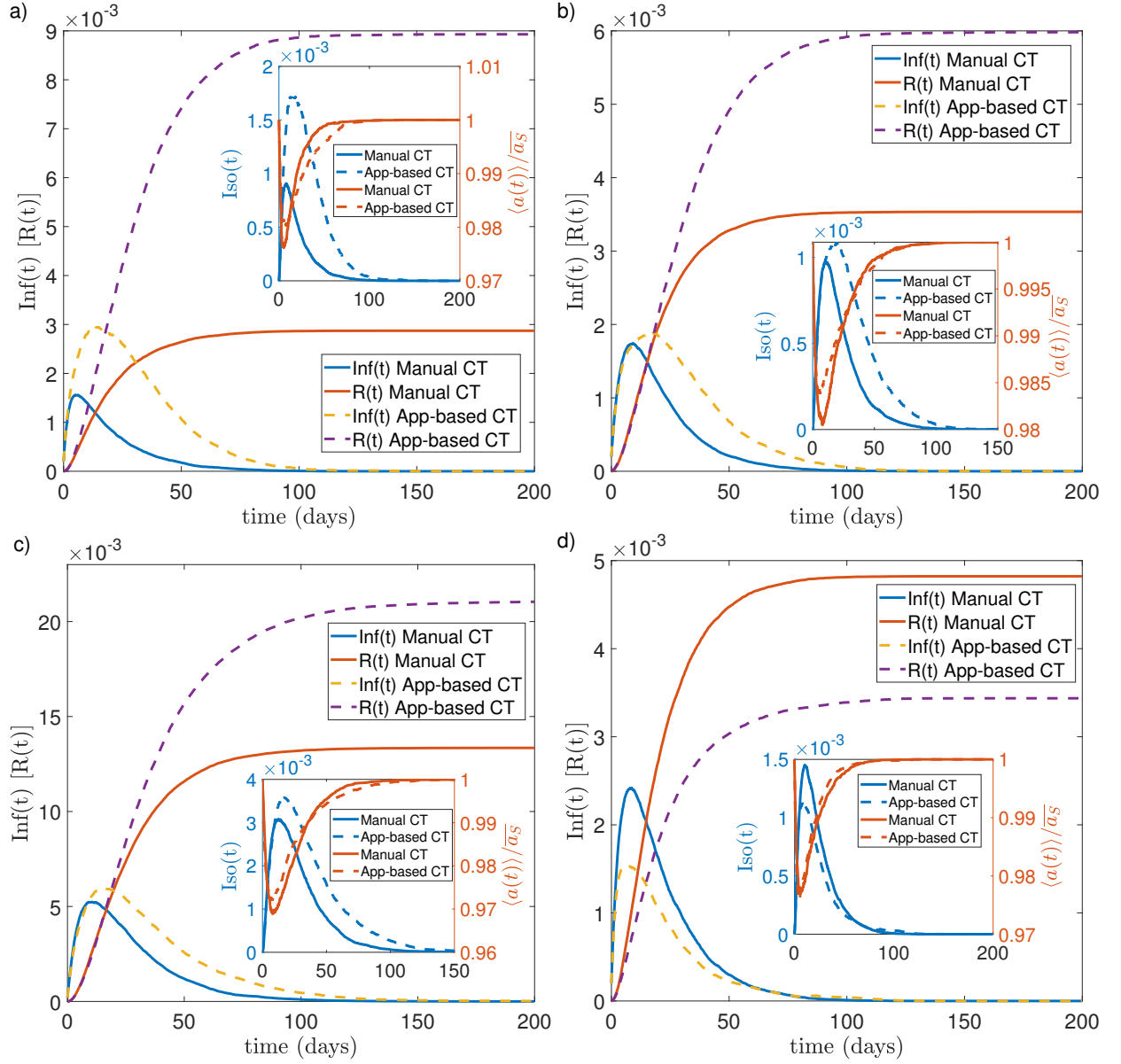


FIG. 2: **Robustness of the results for the epidemic active phase.** In all panels we plot the temporal evolution of the fraction of infected nodes  $Inf(t)$ , i.e. infected asymptomatic and infected symptomatic, and of the fraction of removed nodes  $R(t)$ , for both manual and digital CT. In the insets we plot the temporal evolution of the fraction of isolated nodes  $Iso(t)$  (right y-axis) and of the average activity of the population  $\langle a(t) \rangle$  (left y-axis), normalized with  $\bar{a}_S$ . All curves are averaged on several realization of disorder and temporal evolution. In panel (a) we set  $\tau_C = 0$ ,  $\bar{\epsilon} = f^2 = 0.1$  and  $r/r_C^{NA} = 4.0$ ; in panel (b) we set  $\tau_C = 5$  days,  $\bar{\epsilon} = f^2 = 0.1$  and  $r/r_C^{NA} = 3.1$ ; in panel (c) we set  $\tau_C = 5$  days,  $\bar{\epsilon} = f^2 = 0.1$  and  $r/r_C^{NA} = 7.0$ ; in panel (d) we set  $\tau_C = 5$  days,  $\bar{\epsilon} = f^2 = 0.6$  and  $r/r_C^{NA} = 4.5$ . In all panels  $\rho(a_S, b_S) \sim a_S^{-(\nu+1)} \delta(b_S - a_S)$  with  $a_S \in [a_m, a_M]$ ,  $a_M/a_m = 10^3$ ,  $\nu = 1.5$ ,  $\bar{a}_S = 6.7 \text{ days}^{-1}$ ,  $N = 5 \times 10^3$ ,  $\delta = 0.57$ ,  $\tau_P = 1.5$  days,  $\tau = 14$  days,  $k_c = 130$ ,  $T_{CT} = 14$  days.

- 
- [1] M. Mancastroppa, A. Vezzani, M. A. Muñoz, and R. Burioni, *J. Stat. Mech.: Theory Exp* **2019**, 053502 (2019).
  - [2] M. Tizzani, S. Lenti, E. Ubaldi, A. Vezzani, C. Castellano, and R. Burioni, *Phys. Rev. E* **98**, 062315 (2018).
  - [3] I. Pozzana, K. Sun, and N. Perra, *Phys. Rev. E* **96**, 042310 (2017).
  - [4] G. Ghoshal and P. Holme, *Physica A* **364**, 603 (2006).
  - [5] M. Mancastroppa, R. Burioni, V. Colizza, and A. Vezzani, *Phys. Rev. E* **102**, 020301 (2020).
  - [6] D. T. Gillespie, *J. Comput. Phys.* **22**, 403 (1976).